Contourite distribution and bottom currents in the NW Mediterranean Sea: coupling seafloor geomorphology and hydrodynamic modelling

Elda Miramontes[a*], Pierre Garreau[b], Matthieu Caillaud[c], Gwenael Jouet[a], Romain Pellen[a,d], F. Javier Hernández-Molina[e], Michael A. Clare[f], Antonio Cattaneo[a]

[a] IFREMER, Géosciences Marines, Plouzané 29280, France

[b] UMR 6523 CNRS, IFREMER, IRD, UBO, Laboratoire d'Océanographie Physique et Spatiale, Plouzané 29280, France

[c] IFREMER, Dynamiques des Ecosystèmes Côtiers, Plouzané 29280, France

[d] UMR6538 CNRS-UBO, IUEM, Laboratoire Géosciences Océan, 29280 Plouzané, France

[e] Dept. Earth Sciences, Royal Holloway Univ. London, Egham, Surrey TW20 0EX, United Kingdom

[f] National Oceanography Centre, University of Southampton Waterfront Campus, European Way, Southampton, SO14 3ZH, United Kingdom

*Present address : UMR6538 CNRS-UBO, IUEM, Laboratoire Géosciences Océan, 29280 Plouzané, France

Corresponding author: Elda Miramontes (Elda.Miramontesgarcia@univ-brest.fr)

Abstract

Contourites are common morphological features along continental margins where currents encounter the seafloor. They can provide long-term archives of palaeoceanography, may be prone to sediment instability, and can have a great potential for hydrocarbon exploration. Despite their importance and increasingly recognised ubiquitous occurrence worldwide, the link between oceanographic processes and contourite features is poorly constrained. In particular, it is unclear under which specific conditions sediments are mobilised, modified and deposited by bottom currents. Here, we aim to determine key bottom current characteristics (velocity and bottom shear stress) affecting contourite deposition, by assuming that recent oceanographic regimes may be

extended back in time over the past glacial-interglacial cycles, with strong winter circulation assumed similar to glacial conditions and weak summer circulation to interglacials. We present an integrated study from the NW Mediterranean Sea that couples results of the MARS3D hydrodynamic model with high-resolution sedimentological and geophysical data (piston cores, multibeam bathymetry and high resolution seismic data). Near bottom circulation was modelled during winter and summer 2013 as representative of past periods of high and low current intensity, respectively. Model results match well with the extent of contourite depositional systems and their different localised morphologic elements. We deduce that higher intensity events control the formation of erosional features such as moats and abraded surfaces. The heterogeneous distribution of bottom-current intensity on slopes explains the development of different types of contourite drifts. Plastered drifts form in zones of low bottom-current velocities constrained upslope and downslope by higher current velocities. Separated elongated mounded drifts develop where fast bottom-currents decelerate at foot of the slope. In contrast, no mounded contourite morphologies develop when the current velocity is homogeneous across the slope, especially in margins prone to downslope sediment transport processes. In confined basins, gyres may transport sediment in suspension from a margin with a high sediment supply to an adjacent starved margin, favouring the development of fine-grained contourites in the latter. Our results provide new insights into how detailed bottom-circulation modelling and seafloor geomorphological analyses can improve the understanding of palaeoflow-regimes, at least over time spans when the overall paleogeography and the distribution of contourite drifts is comparable to present-day conditions. The approach of coupled hydrodynamic models and geomorphological interpretations proposed here for depositional, erosional and mixed contourite features may be used to understand other areas affected by bottom currents, and for a better conceptual understanding of bottom-current processes and their interactions with the seafloor.

Keywords

Sediment drift; Along-slope processes; Erosion; Oceanic circulation; Bottom shear stress

1. Introduction

Oceanic currents play a major role in controlling the morphological and sedimentary evolution of continental margins (Rebesco and Camerlenghi, 2008). Bottom current-induced sediment winnowing, remobilisation and erosion sculpt the seafloor on a wide variety of scales, and can have a profound influence on local to regional sediment accumulation rates (Hernández-Molina et al., 2008; Stow et al., 2009). Large contourite sedimentary accumulations are known as “drifts”, which may be more than 100 km wide, hundreds of kilometres long and up to 2 km thick (Stow et al., 2002; Rebesco and Camerlenghi, 2008; Rebesco et al., 2014). As contourite drifts typically have higher sedimentation rates than pelagic sediments, the resultant expanded stratigraphy can provide long-term, high-resolution archives of palaeoceanography and palaeoclimate (Knutz, 2008; McCave, 2008). Due to their depositional geometries, contourites may be prone to instability, thus posing a hazard for seafloor infrastructure (Laberg and Camerlenghi, 2008; Miramontes et al., 2018), and they may be economically viable prospects for hydrocarbon exploration (Viana, 2008).

Contourite drifts are commonly associated with persistent bottom currents related to long-term thermohaline circulation patterns (Stow et al., 2002), although the physical processes that control their formation are still poorly understood due to the paucity of direct observations and modelling studies (Hunter et al., 2007; de Lavergne et al., 2016; Hernández-Molina et al., 2016). Persistent bottom currents can be affected by many intermittent oceanic processes, such as eddies, internal waves, deep-sea storms, rogue waves and/or tsunami related currents (Shanmugam, 2013; Rebesco et al., 2014). In addition, thermohaline circulation is often highly variable at seasonal (Astraldi and Gasparini, 1992), interannual (Pinardi et al., 2015) and geological (thousands to millions of years) timescales (Cacho et al., 2000).

78 The first attempts to explain the effect of bottom currents on sedimentation in deep settings using *in*
79 *situ* measurements were carried out in the 1970's (Gardner et al., 2017; and references therein).
80 However, oceanographic measurements are scarce in deep areas, and they are also limited in time
81 and space (de Lavergne et al., 2016). Numerical modelling thus provides a useful tool to study the
82 interactions between bottom currents and seafloor, since it can cover larger areas and longer periods
83 of time. New advances in modelling submesoscale circulation (scale ranges 0.1–10 km in the
84 horizontal, 0.01–1 km in the vertical, and hours-days in time; McWilliams, 2016) allow the
85 comparison between hydrodynamic modelling and geophysical data. Numerical simulations are a
86 valuable tool to understand the influence of present-day hydrodynamics on sedimentary processes
87 along continental slopes (e.g. Bellacicco et al., 2016; Bonaldo et al., 2016), and have been used to
88 test the effects of different contemporary hydrodynamic processes on contourite systems
89 (Dutkiewicz et al., 2016; Zhang et al., 2016; Thran et al., 2018). However, these modelling studies
90 cannot fully explain the sedimentary processes that control the formation of depositional and
91 erosional contourite features over long time scales. A key outstanding question concerns the relative
92 significance of short-term intensifications in bottom current activity. Are geologically brief periods of
93 extreme near-bed currents the dominant controlling factor on the inception of contourites and
94 correlated seafloor features? Are persistent background conditions more important in shaping
95 distinct depositional architectures instead? To address these questions, it is necessary to integrate
96 calibrated numerical modelling with evidence of past bottom-current activity over geological time
97 scales. In a recent study, Thran et al. (2018) compared at a global scale (low resolution) the extent of
98 known contourite deposits and modelled bottom current velocity, showing an overall matching of
99 the two datasets. Here we examine the output of a high resolution numerical oceanographic model,
100 calibrated on short-term (seasonal) hydrodynamic variations, to propose an explanation of how,
101 where and why contourite-related features may develop or may be sustained by present-day oceanic
102 conditions at the seafloor. We then attempt to extrapolate those results to provide inference on the
103 development of contourites over longer (>millennial) time scales.

In the present study, we examine the output of a high resolution numerical oceanographic model, to propose an explanation for the distribution of contourite-related features in the Northwestern Mediterranean Sea. We focus our study on the NW Mediterranean Sea because: i) the oceanic circulation of this area has been well studied from measurements and numerical modelling (Pinardi et al., 2015; and references therein); ii) it has a well-known seasonal variability (intense circulation in winter and weak in summer; Astraldi and Gasparini, 1992; Artale et al., 1994; Rubio et al., 2009); and, iii) it is a region where many contourites have been identified. Contourites have been identified in the Balearic Sea (Velasco et al., 1996; Vandorpe et al., 2011; Lüdmann et al., 2012), the Ligurian Sea (Soulet et al., 2016; Cattaneo et al., 2017) and the northern Tyrrhenian Sea (Roveri, 2002; Cattaneo et al., 2014; Miramontes et al., 2016). In particular, we focused on three areas of the NW Mediterranean Sea: (1) the Balearic Sea (Liguro-Provençal Basin), (2) the Ligurian Sea (offshore the Portofino Promontory) and (3) the Northern Tyrrhenian Sea (Corsica Trough and a seamount off southeast Corsica; Fig. 1). The aims of this study are to: i) identify how present-day current velocities and bottom shear stresses are spatially distributed with respect to the location of long lasting bottom-current influenced seafloor morphologies and deposits (contourite drifts, seafloor erosion features); ii) explore the contrasted scenarios of contourite drifts as mainly controlled by constant currents of moderate intensity or by short-term events of high intensity; and iii) evaluate how bottom currents might redistribute sediment within a confined basin from a margin with high sediment supply to a starved margin.

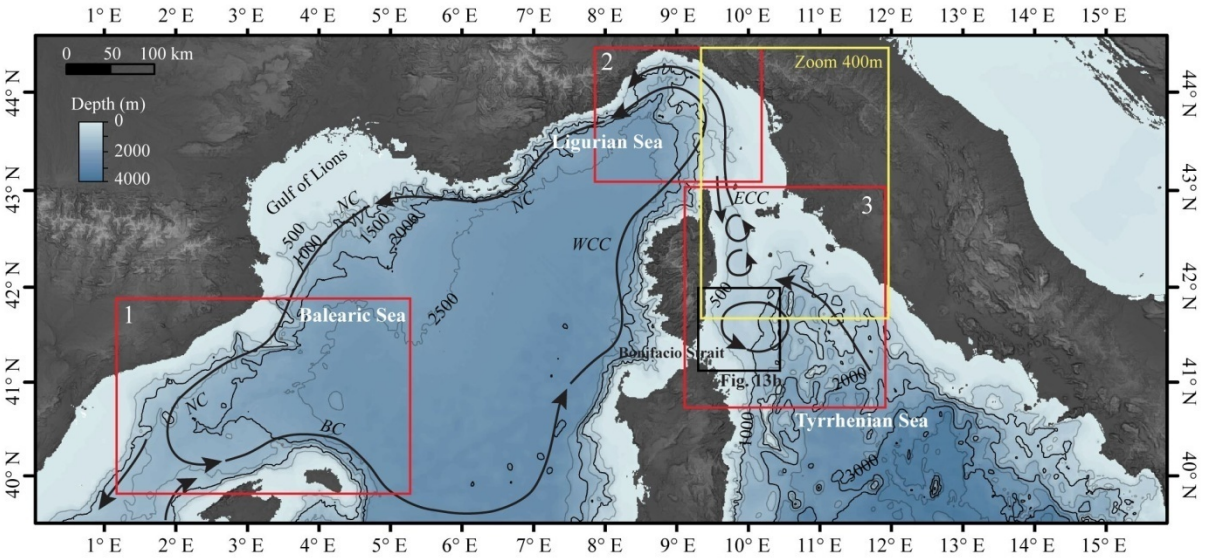

Fig. 1. Bathymetry of the NW Mediterranean Sea (GEBCO) showing the main circulation structures at 200-300 m based on Pinardi et al. (2015) and the present study, and location of the three study areas: 1-Balearic Sea, 2-Ligurian Sea, 3-Northern Tyrrhenian Sea. NC: Northern Current; BC: Balearic Current; WCC: Western Corsica Current; ECC: Eastern Corsica Current. The map shows the extension of the zone simulated with the MARS3D hydrodynamic model in the MENOR configuration (resolution of 1.2 km), and the yellow rectangle shows the location of the zoom of the model simulated with a higher resolution (400 m).

2. Regional setting

The Mediterranean Sea is a mid-latitude semi-enclosed sea connected with the Atlantic Ocean through the Strait of Gibraltar. At present, it has an anti-estuarine circulation (inflow of low salinity surface water and outflow of a deep denser water with high salinity) forced by wind stress and buoyancy fluxes (Pinardi et al., 2015). The negative heat and fresh water budgets of the Mediterranean Sea are balanced over a multidecadal timescale by the entrance of Atlantic Water (AW) through the Strait of Gibraltar (Pinardi et al., 2015). As the AW flows through the Mediterranean Sea, it evolves to a water mass named Modified Atlantic Water (MAW). The MAW is a fresher water mass present in the upper 100-200 m of the water column (Millot and Taupier-Letage, 2005; Millot, 2009). The MAW overlies the Levantine Intermediate Water (LIW), which is formed in

the Levantine Basin by a process of evaporation during the summer and by a winter cooling (Lascaratos et al., 1993; 1999). After passing the Strait of Sicily, the LIW flows northwards along the eastern and western coasts of the Corsica Island as part of the Eastern and Western Corsican Currents (ECC, WCC; Millot et al., 1999; Fig. 1). The ECC can reach current speeds of more than 40 $cm \cdot s^{-1}$ near the surface and more than 20 $cm \cdot s^{-1}$ near the seafloor at the Corsica Strait (Vignudelli et al., 2000). The currents are more intense and with a northwards direction in winter, while in summer they are weaker and occasionally flow southwards (Astraldi and Gasparini, 1992; Vignudelli et al., 2000; Ciuffardi et al., 2016). The ECC (at the depth range of the LIW) is related to the formation of contourite systems in the Corsica Trough (Table 1; Miramontes et al., 2016).

Study area	Current velocity from literature	Water masses	Drift water depth	Water mass at drift location
Balearic Sea	Northern Current (NC): westwards along the Iberian slope. Balearic Current (BC): eastwards along the Balearic Islands (Pinardi et al., 2006). In winter, deep convection and dense shelf water cascading: up to 55 $cm \cdot s^{-1}$ in the continental slope (Palanques et al., 2012; Durrieu de Madron et al., 2017).	MAW (0-200 m), WIW (200-400 m, if present), LIW (400-700 m), WMDW (>700 m) (Salat and Font, 1987; Font et al., 1988).	2000-2700 m	WMDW
Ligurian Sea	Northern Current (NC): westwards; NC more intense (max. 30-50 $cm \cdot s^{-1}$ near the surface), narrower and deeper in winter (Albérola et al., 1995).	MAW (0-150 m), LIW (150-1000 m, when the WIW is not present), WMDW (>1000 m) (Gasparini et al., 1999; Millot et al., 1999).	900 m	LIW
Northern Tyrrhenian Sea	East Corsica Current (ECC): northwards, episodically southwards (in summer); more intense in winter, more than 40 ~~20~~ $cm \cdot s^{-1}$ near the surface and 20 $cm \cdot s^{-1}$ near the seafloor (Vignudelli et al., 2000).	MAW (0-200 m), LIW (200-1000 m), WMDW (>1000 m) (Millot et al., 1999).	170-850 m in the Corsica Trough and 820-900 m in the seamount south of the Corsica Trough.	LIW

Table 1. Summary of the overall current characteristics, water masses distribution, water depth of the studied sediment drifts and identification of the water mass in contact with contourite morphologies in the three study areas: Balearic, Ligurian and Northern Tyrrhenian Seas. MAW: Modified Atlantic Water; WIW: Western Intermediate Water; LIW: Levantine Intermediate Water; WMDW: Western Mediterranean Deep Water.

The ECC and WCC feed the Northern Current (NC), which is a slope current flowing along the Ligurian Sea up to the Balearic Sea (Astraldi et al., 1994; Fig. 1). The NC closes cyclonically in the Balearic Sea, flowing along the northern Balearic margin as the Balearic Current (BC; Pinot et al., 2002; Fig. 1), and

forming part of the Gulf of Lions gyre (Pinardi et al., 2006). The NC also presents a seasonal variability: in summer the NC is weak, wide (about 50 km) and shallow (down to 250 m); while in winter the NC stronger (maximum velocity near the surface of 30-50 $cm \cdot s^{-1}$), narrow (about 30 km) and deep (down to about 450 m) (Albérola et al., 1995). The NC (at the depth range of the LIW) is at the origin of contourite features along the Ligurian margin located at 200-1000 m water depth (Table 1; Soulet et al., 2016; Cattaneo et al., 2017).

The deep part of the NW Mediterranean Sea (below 1000 m water depth) is characterised by the presence of the Western Mediterranean Deep Water (WMDW) (Millot, 1999). This water mass is mainly formed in the Gulf of Lions by surface cooling and evaporation due to cold and dry northern winds, and open-sea convection (Durrieu de Madron et al., 2013). Bottom-reaching convection events can generate intense currents near the seafloor with speeds up to 45 $cm \cdot s^{-1}$, strong enough to locally resuspend sediment (Durrieu de Madron et al., 2017). Dense shelf water cascading also generates strong bottom currents up to 95 $cm \cdot s^{-1}$ in canyons and 40-55 $cm \cdot s^{-1}$ in the slopes. Between January and April, these currents very often erode the seafloor and transport large amount of particles in the bottom layer (Palanques et al., 2012). All these events may affect the formation of contourites in the Balearic Sea. Contourites in this area are located at 2000-2700 m in the depth range of the WMDW (Table 1; Velasco et al., 1996).

3. Materials and methods

3.1. Geophysical, ~~and~~ sedimentological data and terminology

Various bathymetric data sets were used to enable geomorphological analysis and oceanographic modelling, detailed in Table 2. Seismic data were used to characterise the sub-surface architecture of contourite depositional and erosional features. The seismic data set used for this study was acquired with four different types of seismic sources (Table 2).

The piston cores presented in this study were collected along the Pianosa Ridge in 2013 during the PRISME3 cruise (Cattaneo, 2013b) onboard the R/V Pourquoi pas?, and along the Minorca margin in

2018 during the WestMedFlux2 cruise (Poort and Gorini, 2018) onboard the R/V L'Atalante. The cores of the Pianosa Ridge are 9 to 22 m long and were collected between 176 and 342 m water depth, and the core of the Minorca margin is 8 m long and was collected at 2694 m water depth.

The criteria used in the present study to identify contourites and bottom–current related features followed the concepts proposed by Faugères et al. (1999), Faugères and Stow (2008), Nielsen et al. (2008) and Rebesco et al. (2014). In this study we identified two main types of contourite drifts: separated elongated mounded drifts and plastered drifts. Separated elongated mounded drifts are often found on the lower slope, associated with steep slope gradients. They are separated from the slope by a linear depression (a contourite channel, termed 'moat') that can be formed by erosional or non-depositional processes (Rebesco et al., 2014). We mapped their offshore limit as the inflexion point of the slope, where the mounded shape ends. Plastered drifts are typically found on gentle slopes (Faugères and Stow, 2008). They form a convex shape, with the predominance of sediment accumulation in the centre of the drift (Faugères and Stow, 2008). Contourite terraces are flat surfaces commonly associated with plastered drifts, which are often dominated by erosion (Hernández-Molina et al., 2016).

Zone	Bathymetry origin and horizontal resolution	Seismic data
Balearic Sea	GEBCO (GEBCO_08, version 2010-09-27, http://www.gebco.net), 30 arc-second.	Low resolution multi-channel seismic reflection data from VALSIS 2 survey (Mauffret, 1988) and Sub-Bottom Profiler (SBP) data from WestMedFlux2 (Poort and Gorini, 2018).
Ligurian Sea	GEBCO (GEBCO_08, version 2010-09-27, http://www.gebco.net), 30 arc-second.	Deep-towed SYSIF (Système Sismique Fond) seismic reflection data (220-1050 Hz) from PRISME2 survey (Cattaneo, 2013a).
Western and Central Corsica Trough	Multibeam bathymetry from CORFAN (Savoye, 1998), CORFAN 2 (Savoye, 2001) and SIGOLO surveys (Savoye, 2008), 25 m.	48-72-channel sparker seismic reflection data (130-750 Hz) from SIGOLO survey (Savoye, 2008)
Eastern Corsica Trough (Pianosa Ridge)	Multibeam bathymetry from PRISME2 (Cattaneo, 2013a), PAMELA-PAPRICA (Cattaneo and Jouet, 2013) and PRISME3 surveys (Cattaneo, 2013b), 5 and 15 m.	72-channel high resolution mini GI gun seismic reflection (50-250 Hz) and Sub-Bottom Profiler data (SBP, 1800-5300 Hz) from PRISME 2 (Cattaneo, 2013a) and PAMELA-PAPRICA surveys (Cattaneo and Jouet, 2013).
Seamount Northern Tyrrhenian Sea	Multibeam bathymetry from an industrial data set, 30 m; and detailed bathymetry acquired with AUV, 1 m.	Multi-channel ultra-high resolution seismic reflection profile from a sleeve gun array of an industrial data set.
NW Mediterranean Sea in hydrodynamic model	ETOPO2, 1.2 km	-

Zoom in the Northern Tyrrhenian Sea in hydrodynamic model	Compilation of GEBCO bathymetry and multibeam bathymetry of the Corsica Trough, 400 m.	-

Table 2. Geophysical data set (Source for morphobathymetric data: bathymetric grid and reflection seismic profiles) in the three study areas (Balearic, Ligurian and Northern Tyrrhenian Seas) and in areas with detailed analysis in the Northern Tyrrhenian Sea (Corsica Trough, Pianosa Ridge, Northern Tyrrhenian Seamounts).

3.2. Hydrodynamic modelling

The MARS3D (3D hydrodynamical Model for Applications at Regional Scale) model was used to simulate coastal and regional circulation (developed by Lazure and Dumas, 2008; revised by Duhaut et al., 2008). ~~Details on the model are reported in the supplementary materials.~~ For this study we used the "MENOR" configuration of the MARS3D model, which extends from the Balearic Islands to the Gulf of Lions and the Ligurian Sea (longitude: 0°E 16°E, latitude: 39.5°N 44.5°N). The model space has a horizontal resolution of 1.2 km and 60 vertical levels using a generalised sigma coordinates system. Details on the model are reported in the supplementary materials. In this study, we modify the resolution based on the scale of current-related features observed on the seafloor. In the Balearic Sea contourite drifts have a maximum width of 25 km, and the moat is about 5 km wide (Velasco et al., 1996). In contrast, contourites in the northern Tyrrhenian Sea present a smaller size. Sediment drifts are less than 10 km wide, and the moat less than 2 km wide (Miramontes et al., 2016). Therefore, in order to better simulate the oceanographic processes at smaller scale, we increased the resolution of the model to 400 m in the Tyrrhenian Sea. The zone of enhanced (400 m) resolution extends from 9.39°E to 12.33°E and 41.71°N to 43.27°N, covering an area from the east Corsican coast to the Italian coast (Fig. 1). During the simulation the MENOR configuration and the zoom are computed simultaneously. Both~~,~~ the 400 m-resolution zone and the MENOR configuration mutually exchange information (current, temperature and salinity) at each time step. This two-way downscaling approach prevents any inconsistency between the coarser and the finer grids.

We simulated three months of winter (January, February and March) 2013 to represent a period of strong currents, and summer 2013 (July, August, September) to represent a period of weak currents. We chose the year 2013 because it is known that the oceanic circulation was very intense during this winter (Léger et al., 2016). Moreover, an intense observation experiment (HYMEX) conducted in the North Western Mediterranean Sea from summer 2012 to spring 2013 provided valuable calibration, enabling robust definition of initial and boundary conditions (Léger et al., 2016). Simulations were thus extended to include a 4 month-long interval prior to the period of interest to assess the model against HYMEX results (i.e. calculations started in September 2012 to have a more realistic initial condition in January 2013). More details on the hydrodynamic model assessment are shown in the supplementary materials.

For the present study we were interested in the near-bed circulation to study the current-seafloor interaction. Therefore, we calculated the bottom shear stress generated by currents at the seafloor based on the model results. At the bed interface the shear stress (τ) is mostly turbulent and can be related to the sea water density (ρ) and the friction velocity (u*) using:

$$\tau = \rho\, u^{*2} \quad (1)$$

In the boundary layer with a steady current, the turbulent velocity can be deduced from the current speed near the bottom with the relation:

$$u^* = \frac{\kappa \cdot u(z)}{\ln\left(\frac{z}{z_0}\right)} \quad (2)$$

where κ is the Von Karman constant (equal to 0.4; Schlichting, 1962), z_0 the bottom roughness length taken here to a constant equal to 0.0035 m and z the distance from the bottom where the current velocity $u(z)$ is computed. The bottom shear stress (BSS) is computed over the thickness of the bottom layer. The use of the bottom stress overcomes the difference in the bottom layer thickness due to the generalised sigma coordinate. In this model we used 60 vertical sigma-levels that are parallel to the topography, therefore the cells are stretched in zones of deeper water, and squeezed where water depths are shallower. We used the 90th percentile of the bottom shear stress in order to

remove the extreme and transitory events. 75th percentiles, median or even mean values were also examined without significant changes in resulting patterns.

The Brunt-Väisälä frequency (or buoyancy frequency, *N*), is the oscillation frequency of a water parcel displaced vertically in a statically stable environment, and it provides information about the water stratification (Da Silva et al., 2009). A layer of high Brunt-Väisälä frequency acts in the fluid as a focus of internal waves, and is an area of potential oscillatory current. It was used in the Corsica Trough to show the zone where internal waves could be formed. It was calculated from the modelled vertical oceanic density gradient according to:

$$N = \sqrt{\frac{g}{\rho}\frac{\partial \rho}{\partial z}} \quad (3)$$

where g is the gravitational acceleration, ρ is the density and $\frac{\partial \rho}{\partial z}$ is the vertical oceanic density gradient.

3.3. Coupling hydrodynamic modeling on short timescales (seasons) and long term sediment erosion/deposition

The locations where contourites have developed in the study areas have not changed significantly since their onset. Contourites started to develop in the Corsica Trough in the Middle-Late Pliocene (2.5-3.5 Ma ago) (Roveri, 2002; Miramontes et al., 2016). There is clear evidence for long-lived contour current activity throughout the Pliocene-Quaternary from seismic data, with remarkable consistent gross deposit architecture and orientations (e.g. Roveri, 2002). These observations suggest that the direction and location of bottom currents have not significantly changed during the same timescales. Although the general circulation pattern in the NW Mediterranean Sea may not have dramatically changed since the Pliocene, the intensity of the bottom currents has changed cyclically. The intermediate and deep bottom currents in the Mediterranean Sea were more intense during sea level low-stands, or colder stages, than during sea level high-stands, or warmer stages (Cacho et al., 2000; Toucanne et al., 2012; Minto'o et al., 2015). Therefore during sea level low-stands, bottom

currents affected the contourite depositional systems by enhanced erosion and emplacement of coarser deposits (Miramontes et al., 2016).

Modelling past oceanic circulation is hampered by the lack of valid boundary conditions. Therefore, we modelled the oceanic circulation during the winter and the summer seasons of 2013 as two representations of intense (winter) and weak (summer) oceanic circulation. Given the correlation of areas of high shear stress under winter conditions with major erosional features, we hypothesize that the circulation pattern during sea level low-stands could be similar to the present-day winter season.

4. Results

4.1. Balearic Sea (Liguro-Provençal Basin)

The Balearic Sea is located between the north of the Balearic Islands and the Iberian Peninsula, with water depths decreasing westward from 2500 m to 1000 m (Fig. 1). The modelled circulation shows the same general patterns during winter and summer 2013. Bottom currents flow westwards along the Iberian slope. They turn cyclonically due to the bathymetric and hydrologic constraints of the basin, flowing back eastwards along the northern Balearic slope (Fig. 2). Modelling of conditions during winter 2013 show dense shelf waters cascading downslope at the western output of the Gulf of Lions and then flowing along the Iberian slope (see Supplementary materials), in agreement with modelling results by Estournel et al. (2016). During that period of time, high mean velocities (20-30 $cm \cdot s^{-1}$; Fig. 2a) and high P90 BSS (90th percentile of the Bottom Shear Stress; > 0.2 $N \cdot m^{-2}$) are obtained across a large part of the Iberian slope (Fig. 2b). During winter, bottom currents are relatively vigorous along the continental slope of the Minorca Basin, especially in the lower slope between 1000 and 2000 m water depth (wd), with mean velocities ranging between 15 and 25 $cm \cdot s^{-1}$ and P90 BSS 0.1-0.2 $N \cdot m^{-2}$. This circulation along the Minorca slope corresponds to the southwards outflow of WMDW formed during winter (Millot, 1999). Bottom currents remain relatively active along the Minorca slope also in summer, with mean velocities of 10-20 $cm \cdot s^{-1}$ (Fig. 2c) and P90 BSS of

0.07-0.2 N·m^{-2} (Fig. 2d). In contrast, in the Iberian slope the circulation near the seafloor is much weaker during summer with mean velocities <10 cm·s^{-1} (Fig. 2c) and P90 BSS <0.03 N·m^{-2} (Fig. 2d).

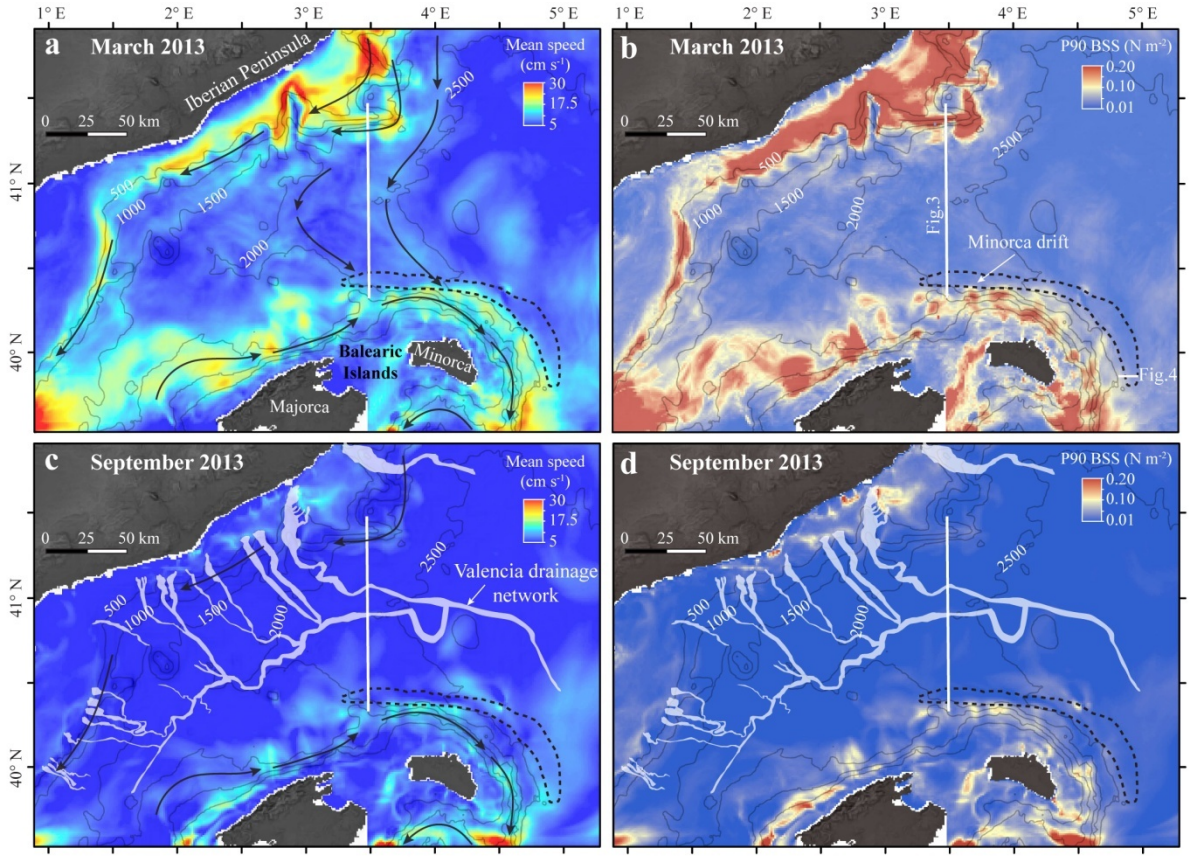

Fig. 2. Results of the MENOR model (cell size of 1.2 km) in the Balearic Sea: during March 2013, (a) mean speed and (b) 90th percentile of the Bottom Shear Stress (P90 BSS); during September 2013, (c) mean speed and (d) P90 BSS. The arrows represent the current direction. The Valencia drainage network is represented with white polygons (adapted from Amblas et al., 2011), and contourite drifts are outlined with dashed lines.

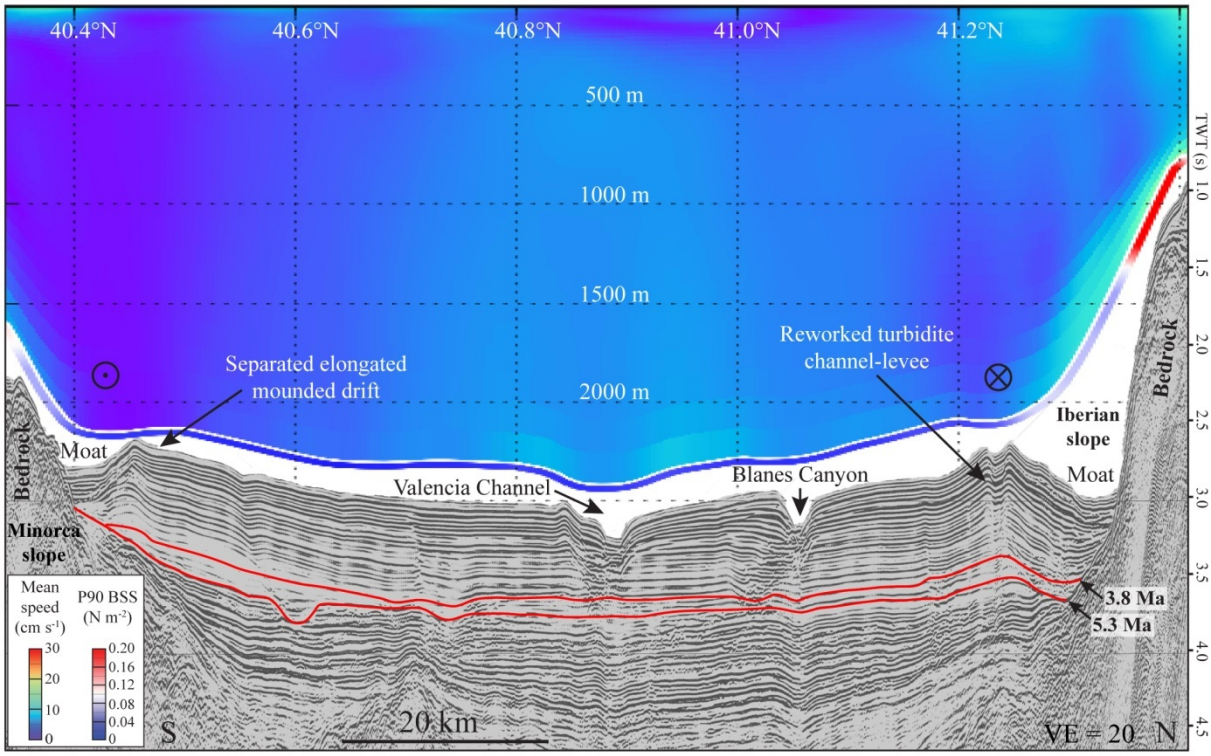

Fig. 3. Seismic reflection profile (VALS88-808) and transect at the same position of the mean speed (~~main surface~~ upper coloured plot) and 90th percentile of the BSS (bottom layer of the coloured plot) from the MENOR model during March 2013. See Fig. 2 for location. Note that the bathymetry used for the hydrodynamic model is a simplified bathymetry with a 1.2 km resolution and thus it does not perfectly fit with the seismic profile. The transect of the model and the seismic profile are not represented at the same depth to avoid overlapping between the images. The red lines represent the boundaries of the onset of the contourite development (based on Rabineau et al. (2014) and Leroux et al. (2017)). Note the two moats at the foot of the continental slope. To the South the moat is adjacent to the Minorca elongated separated mounded drift. To the North the moat erodes part of a turbiditic channel/levee system. ~~See Fig. 2 for location.~~

The morphology of the seafloor between the Iberian and the Minorca slopes is characterized by the presence of erosional features at the foot of the slope that are about 4 km wide, with an incision of about 260 m at 2250 m wd in the Iberian slope, and 150 at 2100 m wd m in the Minorca slope (Fig. 3). North of Minorca this feature can be interpreted as a moat associated with the Minorca sediment drift (dashed line, Fig. 2). The water depth at which the Minorca drift is located increases eastwards,

and the height of the drift decreases in the same direction (Fig. 2; Velasco et al., 1996). The Minorca drift has a convex, arcuate morphology and presents the diagnostic shape of a separated elongated mounded drift on the northern and eastern sides of Minorca (Figs. 3 and 4a). A Sub-Bottom Profiler (SBP) image of the Minorca slope and foot of the slope shows typical contouritic features: (1) an eroded slope characterised by truncated reflections; (2) chaotic acoustic facies of strong amplitude in the moat, suggesting the presence of sediment coarser than on the drift (see core WMF2-KS01 in Fig. 4b); and (3) mounded continuous reflections commonly found in muddy drifts with thin silt layers (Fig. 4). Along the Iberian slope the construction of sedimentary bodies shows the morphology of a turbidite channel with pronounced levees north of the ~~Valencia and the~~ Blanes ~~c~~Canyon~~s~~ (Fig. 3; Amblas et al., 2011). A closer examination of the northern levee reveals an asymmetry in the levee and a flat surface at the foot of the slope (interpreted as a moat), probably due to enhanced erosion by bottom currents at the base of the slope (Fig. 3). The slopes of both Iberian and Minorca margins are strongly eroded, as indicated by exposed bedrock at the seafloor, in agreement with the high modelled P90 BSS (Fig. 3). Separated elongated mounded drifts develop in the zone where bottom currents are relatively weak, with mean velocities below 7 cm·s^{-1} and P90 BSS below 0.03 N·m^{-2} (Figs. 2 and 3; Table ~~2~~3).

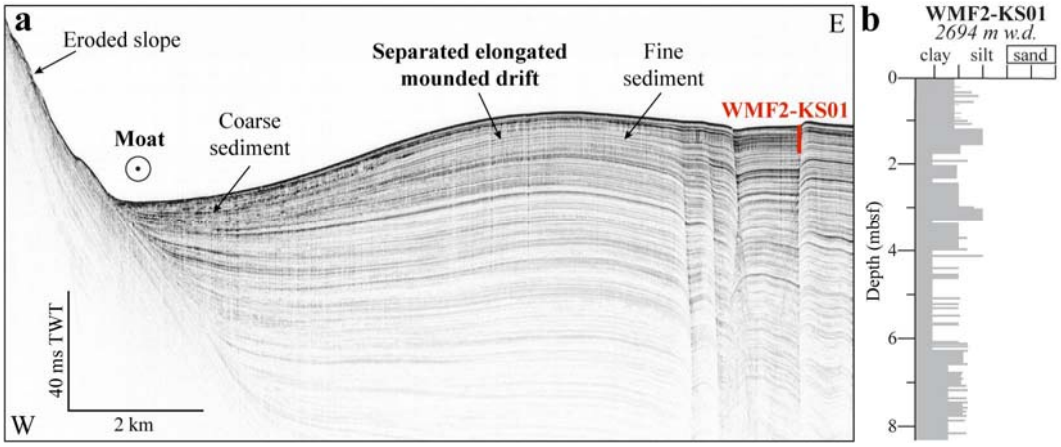

Fig. 4. (a) ~~WMF2018-AT0006B~~ ~~s~~Sub-bottom profiler image (WMF2018-AT0006B) of the southern part of the Minorca drift showing the convex morphology and convergent seismic reflections diagnostic of

a contourite drift and the location of core WMF2-KS01. See Fig. 2b for location. (b) Sediment log of core WMF2-KS01.

4.2. Ligurian Sea

Bottom currents flow northwards and westwards along the Ligurian slope during winter and summer 2013. Currents are vigorous on the continental shelf during winter (related to the MAW) with mean bottom velocities ranging between 15 and 20 $cm \cdot s^{-1}$ (Fig. 5a) and P90 BSS of 0.2-0.4 $N \cdot m^{-2}$ (Fig. 5b). Similar values are found related to the LIW between 600 and 800 m wd offshore Portofino, although in this area P90 BSS is lower; between 0.1 and 0.2 $N \cdot m^{-2}$ (Fig. 5b). In summer, bottom currents on the shelf become less active, with mean velocities <7 $cm \cdot s^{-1}$ (Fig. 5c) and P90 BSS <0.04 $N \cdot m^{-2}$ (Fig. 5d), but they remain important on the slope between 400 and 1000 m wd with mean velocities between 10 and 15 $cm \cdot s^{-1}$ (Fig. 5c) and P90 BSS between 0.06 and 0.13 $N \cdot m^{-2}$ (Fig. 5d). Contourite features are related to this zone of permanent vigorous currents. A separated elongated mounded drift developed in the adjacent deeper zone with lower currents at about 900 m wd, that corresponds to the depth of the drift crest (Fig. 6). The separated elongated mounded drift is mainly composed of mud (Cattaneo et al., 2017). Plastered drifts have been identified by Soulet et al. (2016) and Cattaneo et al. (2017) at 200-600 m in the zone of weaker currents located between two zones of intense bottom currents, as indicated by the model during winter (Fig. 5a). Off Portofino, Cattaneo et al. (2017) also identified a contourite terrace in a zone where modelled bottom currents are strong, 12-17 $cm \cdot s^{-1}$ in winter (Fig. 5a,b).

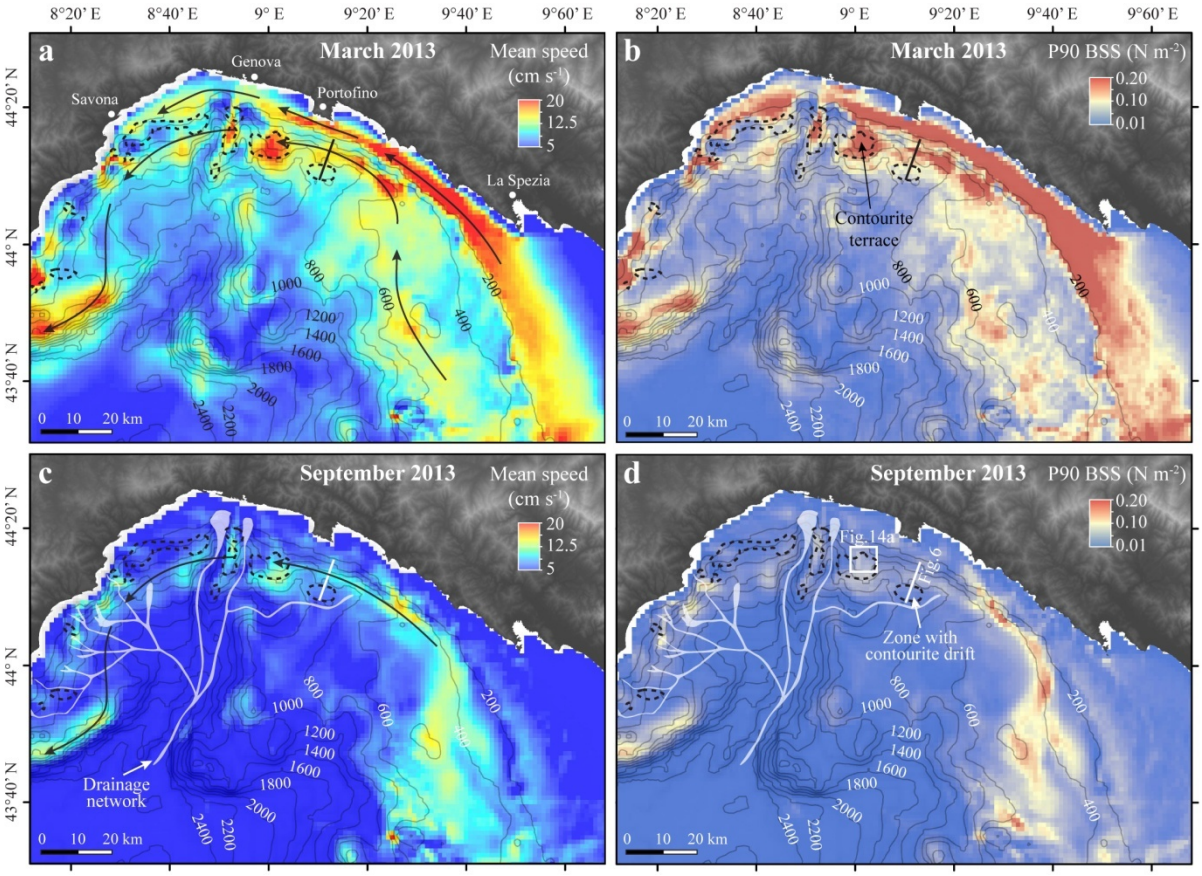

364

365 **Fig. 5.** Results of the MENOR model (cell size of 1.2 km) in the Ligurian Sea: during March 2013, (a)
366 mean speed and (b) 90th percentile of the Bottom Shear Stress (P90 BSS); during September 2013,
367 (c) mean speed and (d) P90 BSS. The arrows represent the current direction. The drainage network is
368 represented with white polygons, and contourite drifts are outlined with dashed lines (adapted from
369 Soulet et al., 2016 and Cattaneo et al., 2017).

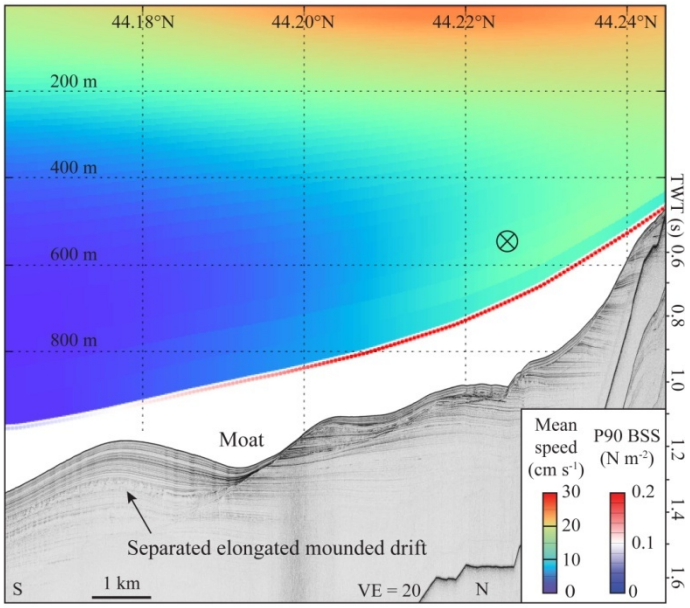

370

371 **Fig. 6.** Deep-towed SYSIF seismic reflection profile (PSM2-15B-PL07-PR01) and transect at the same
372 position of the mean speed (~~main surface~~ upper coloured plot) and 90th percentile of the bottom
373 shear stress (bottom layer of the coloured plot) from the MENOR model during March 2013. Note
374 that the bathymetry used for the hydrodynamic model is a simplified bathymetry with a 1.2 km
375 resolution and thus it does not perfectly fit with the seismic profile. The transect of the model and
376 the seismic profile are not represented at the same depth to avoid overlapping between the images.
377 See Fig. 5 for location.

378

379 4.3. Northern Tyrrhenian Sea

380 Bottom currents in the Corsica Trough are mainly dominated by two cyclonic gyres in the middle of
381 the basin; one offshore the Elba Island and one at about 42°20'N, as well as by alongslope currents
382 flowing northwards along the eastern margin (Pianosa Ridge) and southwards along the western
383 slope (Fig. 7). This circulation pattern is the direct consequence of the seafloor morphology. Bottom
384 currents are weak on the shelf, on the central part of the basin and on the Pianosa Ridge during
385 summer, as the northwards total flux through the strait halts or even reverses in this season (Fig. 7;
386 Vignudelli et al., 2000). Bottom-current velocities increase during summer along the Corsican slope

due to an enhanced entrance of water from the Ligurian Sea southwards into the Corsica Trough (Fig. 7c).

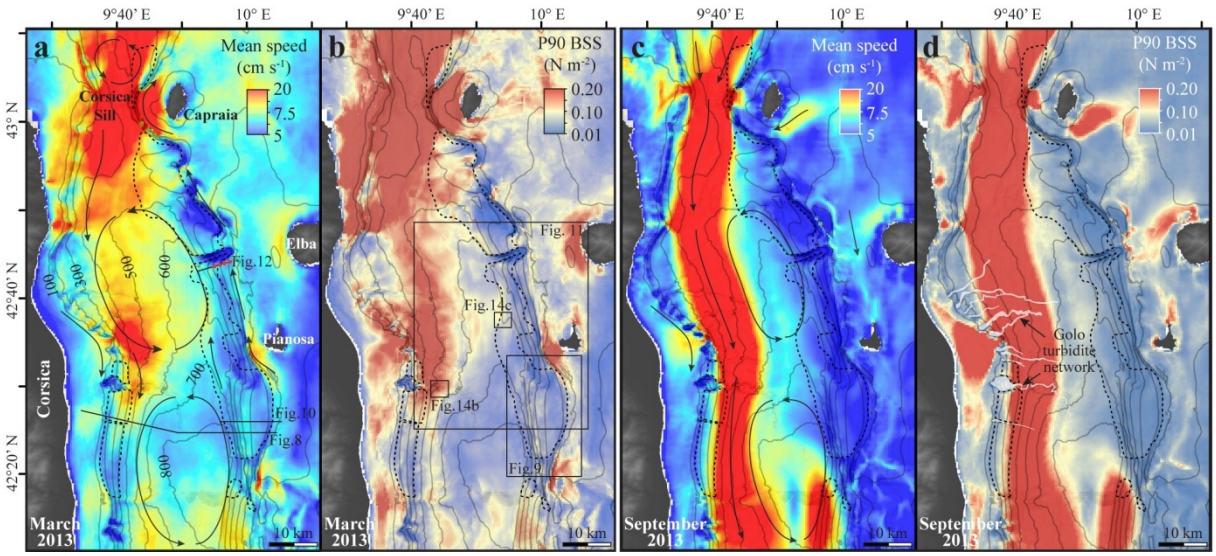

Fig. 7. Results of the MENOR model (zoom with cell size of 400 m) in the Corsica Trough: during March 2013, (a) mean speed and (b) 90th percentile of the Bottom Shear Stress (P90 BSS); during September 2013, (c) mean speed and (d) P90 BSS. The arrows represent the current direction near the seafloor. Contourite drifts are outlined with dashed lines, and the Golo turbidite network is represented with white polygons. Isobaths are represented every 100 m, starting at 100 m water depth. Red dots in Figure 7a represent the location of piston cores.

4.3.1. Eastern slope of the Corsica Trough

Pianosa Ridge

The Pianosa Ridge presents a wide range of drift morphologies. The southern slope, located to the south of the Pianosa Island, is mainly dominated by a plastered drift, a convex-shaped sediment deposit that extends between 150 and 700 m wd (Figs. 8, 9 and 10). The drift is characterised by a contourite terrace in the upper part with lower sedimentary accumulation and lower slope gradients landward. In a seaward direction, a zone of highest sedimentary accumulation occurs on the middle slope (Fig. 10). The hydrodynamic model shows that during the month of March 2013, bottom currents are weaker (mean velocity of 7 cm·s^{-1} and P90 BSS of 0.04 N·m^{-2}) in the middle and lower

406 slope than in the distal part of the lower slope, foot of the slope and shelf edge (Figs. 8 and 9). In the
407 lower slope and below 400 m wd bottom currents are faster during the same period, with mean
408 velocity of 10 cm·s^{-1} and P90 BSS of 0.08 N·m^{-2}. Similar values are found at the shelf edge. Therefore,
409 the zone of the plastered drift development is in an area of weaker currents constrained upslope and
410 downslope by two areas of stronger currents. Besides the differences in speed, the direction of the
411 currents is also different in the zone of the plastered drift. At the shelf edge and at the lower slope
412 bottom currents flow northwards alongslope, thus presenting a higher meridional (N-S) component
413 of the velocity (Fig. 9). Conversely, the bottom currents show a mainly across-slope direction along
414 the plastered drift; west-northwestwards in the middle slope and southeastwards in the upper slope
415 (Fig. 9). The modelled Brunt-Väisälä frequency (a measure of oceanic stratification) in March 2013 is
416 higher along the contourite terrace (Fig. 8c). The terrace zone is thus potentially more affected by
417 internal waves. In summer, the Brunt-Väisälä frequency is only high near the sea surface; therefore,
418 the plastered drift would be less affected by internal waves than in winter (Fig. 8a). Bottom currents
419 have generated erosional features, such as moats on the lower slope, which become deeper
420 northwards (Miramontes et al., 2016). In plan view, these incisions are oriented north-northeast (Fig.
421 9a). North of the plastered drift, the separated elongated mounded drift is bounded from the shelf
422 by an abraded surface; a zone almost devoid of Pliocene-Quaternary sediment (~~Fig. 8a;~~ Miramontes
423 et al., 2016). The model shows that this area is at present under the influence of weak near-bed
424 currents. The modelled bottom currents are consistent with the presence in this area of a thin layer
425 of Holocene muddy sediment, deposited directly on the Messinian surface (Miramontes et al., 2016).
426 Therefore, the present-day currents in this area are weak but this zone was apparently under erosive
427 conditions in the past due to enhanced bottom currents.

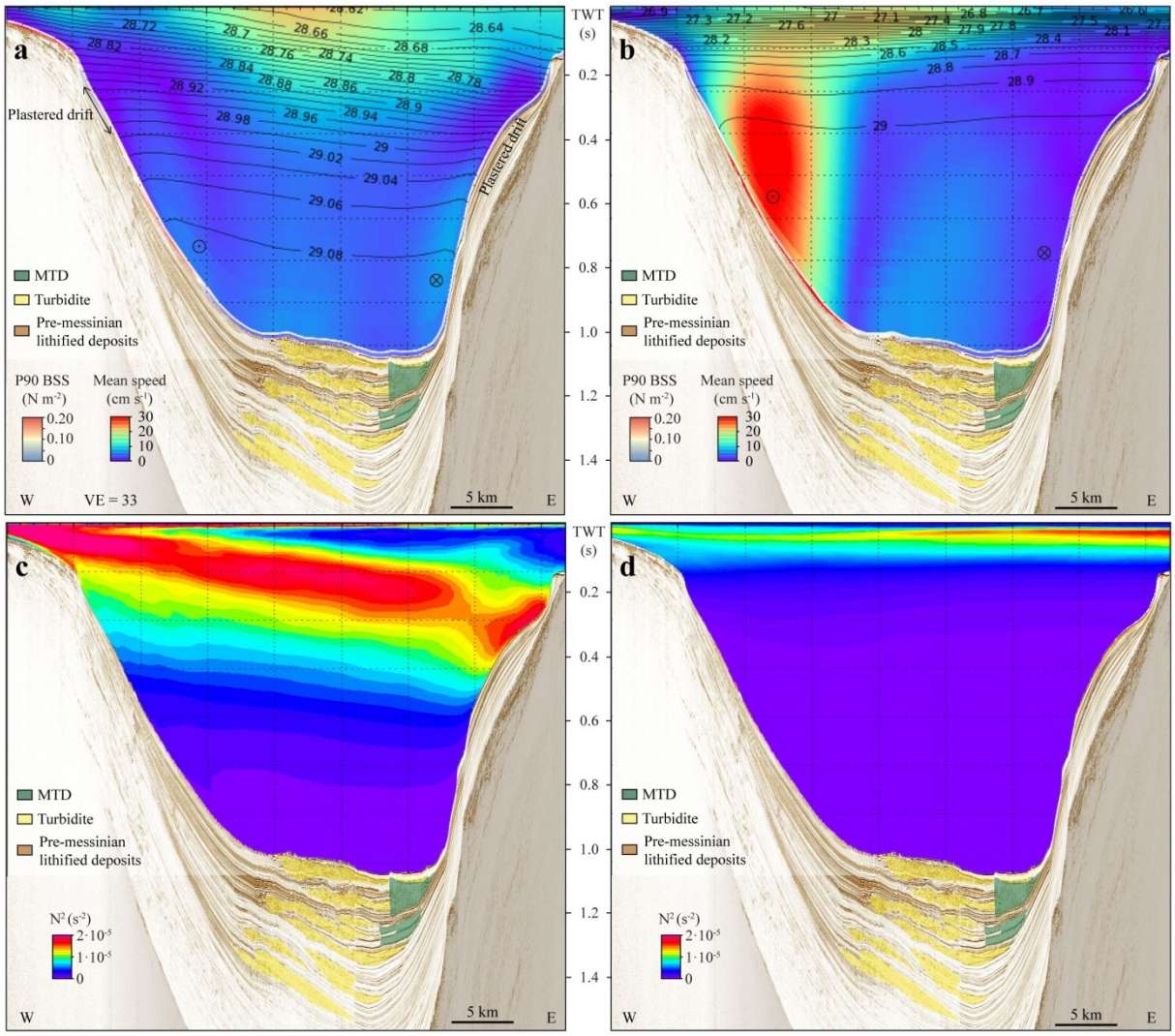

Fig. 8. Composite of multi-channel high resolution mini GI gun seismic reflection profiles (Sigolo-MC069, Sigolo-MC054 and PSM2-HR033) coupled with a transect at the same position from of the MENOR model (zoom 400 m): mean speed (main surface plot) and 90th percentile of the bottom shear stress (bottom layer of the plot) and isopycnal lines (kg·m^{-3}) during (a) March 2013 and (b) September 2013; and Brunt-Väisälä frequency squared (N^2) during (c) March 2013 and (d) September 2013. MTD: Mass Transport Deposit. See Fig. 7a for location.

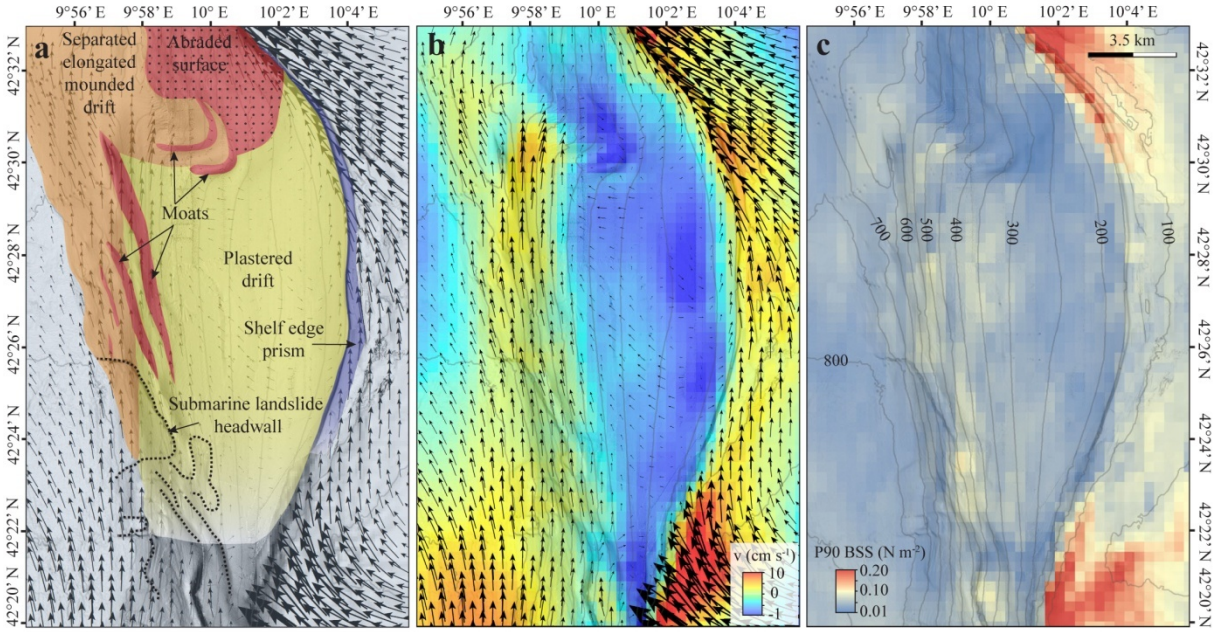

435

436 **Fig. 9.** Zoom on the southern part of the Pianosa Ridge showing the results of the 400 m zoom of the
437 MENOR model during March 2013: (a) Morphosedimentary map showing the location of the main
438 depositional and erosive features, and vectors of the mean velocity current; (b) meridional
439 component of the mean velocity and vectors of the mean velocity current; (c) 90th percentile of the
440 bottom shear stress. See Fig. 7b for location.

441

442

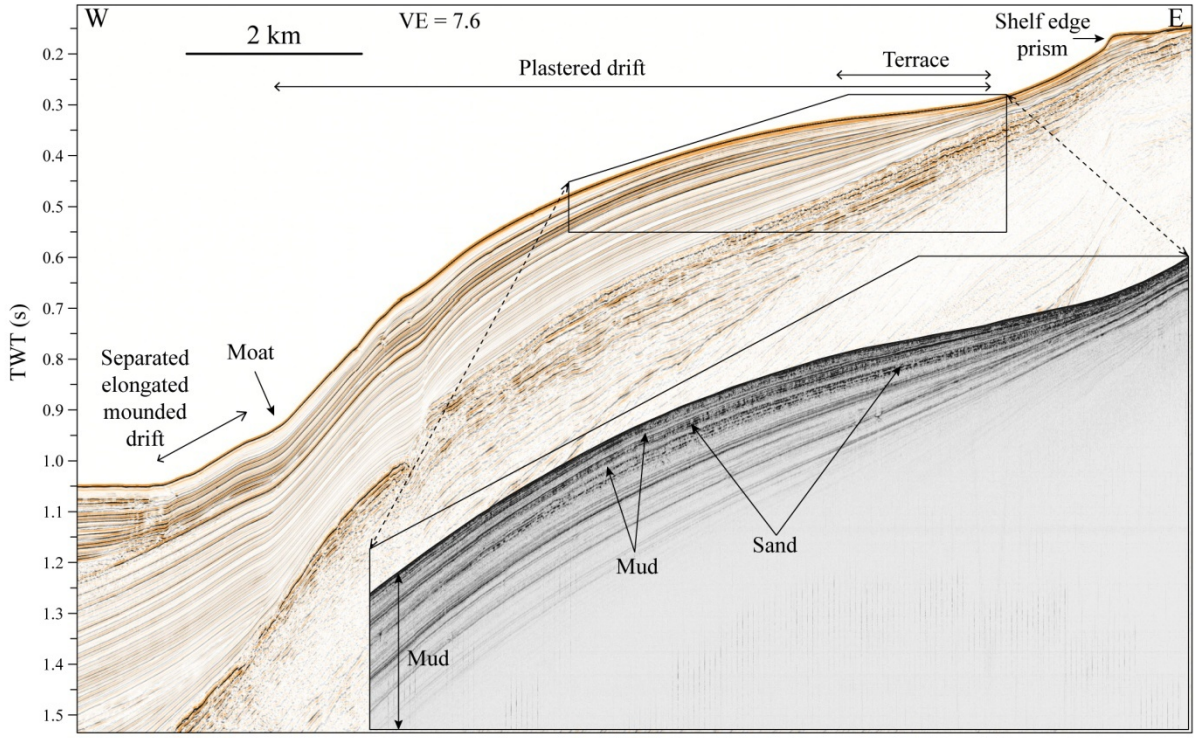

Fig. 10. ~~PSM2-HR-068~~ ~~m~~Multi-channel high resolution mini GI gun seismic reflection profile (PSM2-HR-068) and ~~PSM2-CH-068-S~~ sub-bottom profiler image (PSM2-CH-068) showing a plastered drift characterised by sandy material in the upper and proximal part, and muddy sediment in the lower and more distal part. See Fig. 7a for location.

Pianosa Island-Elba canyon

Further north, between the Pianosa Island and ~~the~~ Elba Canyon, the drift morphology changes ~~between the Pianosa Island and the Elba Canyon~~, and the slope is dominated by multicrested drifts, which are separated from the shelf edge by an eroded zone (Fig. 11). The crests have variable orientations. To the south there is a single NE-SW-orientated crest, while to the north the crests are multiple and parallel, presenting a NW-SE orientation. The moats that separate these crests have an NW-SE orientation. The variable crest orientation can be explained with the circulation pattern near the seafloor during winter. In the central part of the basin there is a cyclonic gyre that affects the lower slope and forms the crest with the NE-SW orientation ~~(Fig. 11)~~. The alongslope currents flowing towards the north at 500-700 m wd affect the shallower part of the NE-SW-oriented crest.

Therefore, the drift crest with a NE-SW orientation is the result of predominantly depositional processes in a zone of slower currents between a cyclonic gyre and alongslope currents ~~(Fig. 11)~~. The multicrested drifts with a NW-SE orientation are related to the alongslope bottom currents. In the upper slope, where seismic data show a zone of erosion, the model indicates fast currents during winter of 7-10 $cm \cdot s^{-1}$ and P90 BSS of 0.05-0.1 $N \cdot m^{-2}$ ~~(Fig. 11)~~.

Faster bottom currents at the shelf edge and at the upper slope favour the transport of sandy material from the shelf to the upper slope and the winnowing of fine material from the latter. Therefore, in the zone of the multicrested drifts, the grain size and the abundance of sediment layers with coarse material decrease with depth (Fig. 12). The sandy sediment is characterised by chaotic acoustic facies of high amplitude on seismic sub-bottom profiles (Fig. 12). Similar acoustic facies can be found in the upper and middle part of the plastered drift (Fig. 10) and in the moat of the Minorca drift (Fig. 4). The terrace located in the upper part of the plastered drift is mainly composed of sand, while in the middle part the sandy layers are interbedded with muddy sediment and in the lower part the plastered drift is mainly composed of mud (Fig. 10).

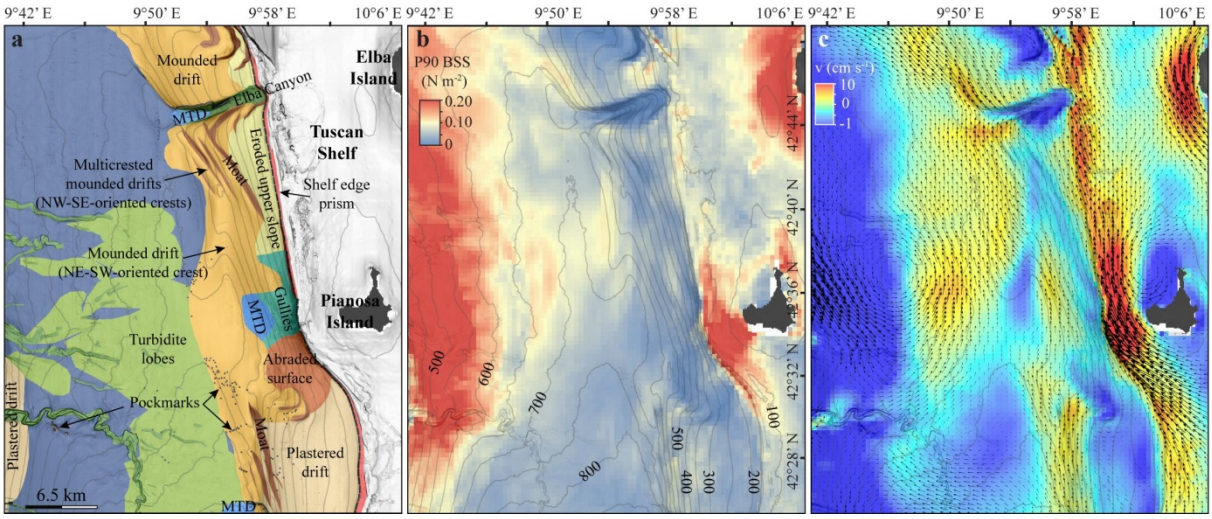

Fig. 11. Zoom on the northern part of the Pianosa Ridge showing the results of the 400 m zoom of the MENOR model during March 2013: (a) morphosedimentary map showing the location of the main depositional and erosive features; (b) 90th percentile of the bottom shear stress; (c) meridional

component of the mean velocity and vectors of the mean velocity current. MTD: Mass Transport Deposit. See Fig. 7b for location.

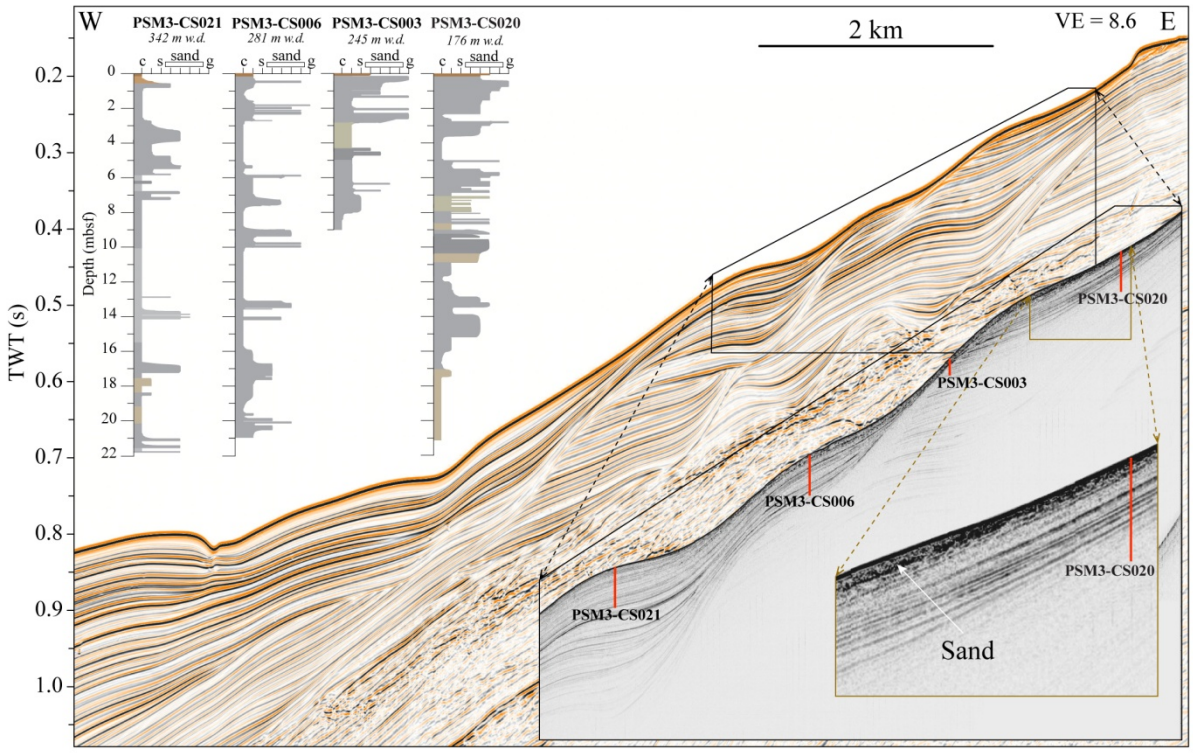

Fig. 12. ~~PSM2-HR-054~~ ~~m~~Multi-channel high resolution mini GI gun seismic reflection profile (PSM2-HR-054) and ~~PSM2-CH-054~~ ~~S~~ sub-bottom profiler image (PSM2-CH-054) showing multicrested mounded drifts, sampled by 4 Calypso piston cores (sediment logs are shown on the left of the figure). Note that the sediment is coarser in the upper slope. See Fig. 7a for seismic profile and core locations.

4.3.2. Western slope of the Corsica Trough

Bottom currents flow southwards along the western margin of the Corsica Trough. Model results show mean velocities that can be higher than 20 $cm \cdot s^{-1}$ and P90 BSS higher than 0.20 $N \cdot m^{-2}$ in summer and in winter (Fig. 7). Bottom currents are weaker on the upper slope with mean velocities of 7-12 $cm \cdot s^{-1}$ and P90 SS of 0.08-0.14 $N \cdot m^{-2}$ both summer and winter (Fig. 7). A small plastered drift is located in this area of weak currents in the upper part of the slope at 160-400 m wd (Figs. 7 and 8).

493 4.3.3. Seamount south of the Corsica Trough

494 The bottom circulation around the seamount located at the south of the Corsica Trough, off
495 southeast Corsica (Fig. 1) is clockwise, and the BSS can be intense in winter, reaching up to 0.05-0.1
496 N-m^{-2} (Fig. 13). Separated elongated mounded drifts are situated at the east of the seamount at the
497 foot of the slope, where the results of the model show southwards bottom currents (Fig. 13). The
498 modelled strong currents explain the reduced sedimentation around the seamount, with a thickness
499 of only 20-50 m during the last 5.3 Ma (Fig. 13c).

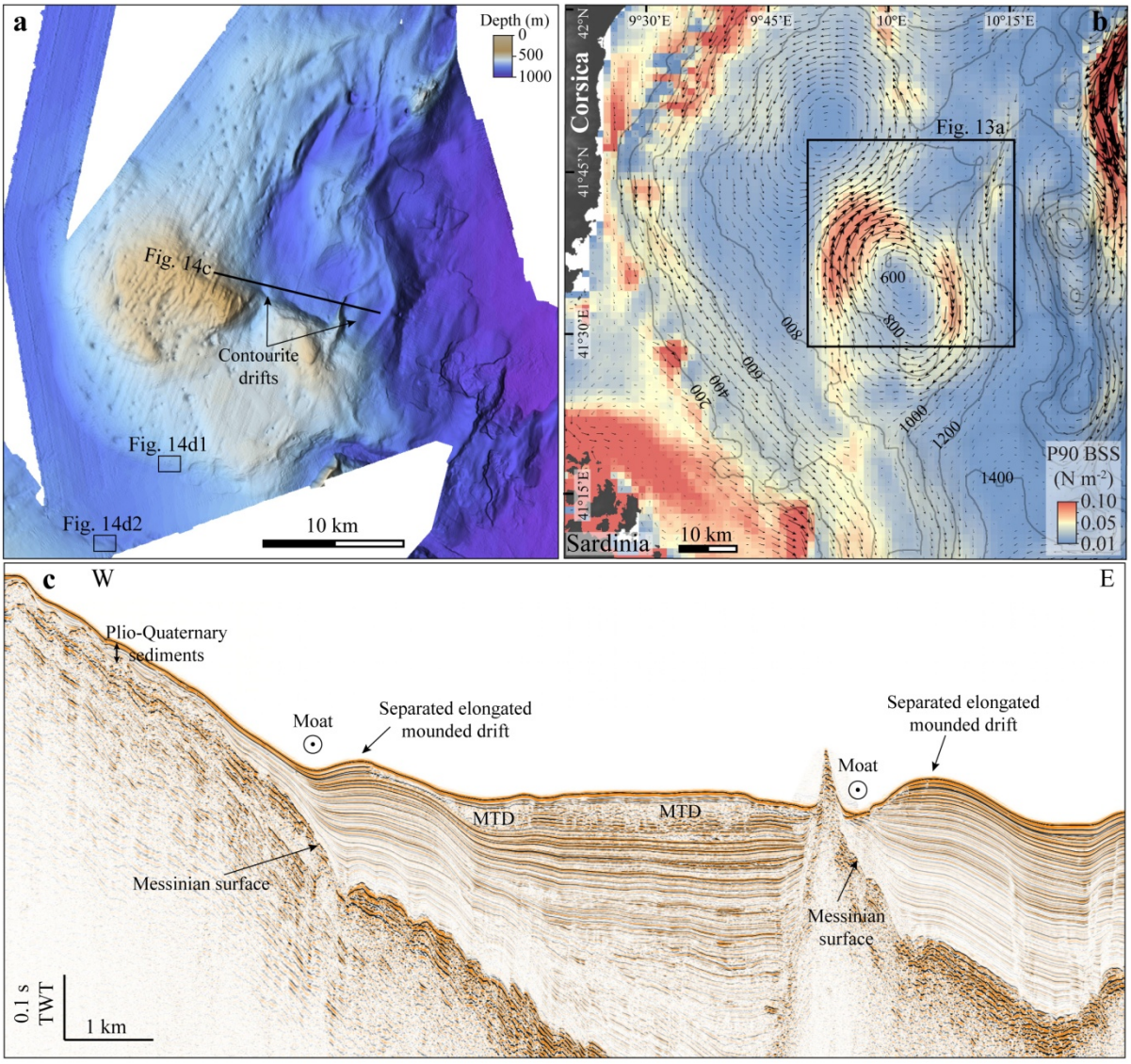

500

501 **Fig. 13.** (a) Multibeam bathymetry of a seamount in the Northern Tyrrhenian Sea with associated
502 contourite drifts. (b) 90th percentile of the bottom shear stress and vectors of the mean velocity

503 during winter 2013 from the MENOR model. See Fig. 1 for location. (c) Multi-channel high resolution
504 seismic reflection profile showing two contourite drifts. MTD: Mass Transport Deposit.
505
506 4.4. Elongated pockmarks as bottom-current indicators
507 The morphologic asymmetry of pockmarks has been proven to be in agreement with bottom current
508 direction and thus to be a useful tool to support modelling of near-seafloor circulation (Schattner et
509 al., 2016; Picard et al., 2018). Pockmarks formed as a result of seafloor fluid expulsion are abundant
510 in many parts of the NW Mediterranean Sea (Riboulot et al., 2014; Cattaneo et al., 2017). The
511 morphology of these seafloor depressions is locally elongated parallel to the direction of dominant
512 bottom currents in the Ligurian and the Northern Tyrrhenian Seas (Fig. 14). In section, pockmarks
513 show a steep flank upstream and a flat eroded flank downstream. A mounded sediment deposit,
514 separated from the pockmark flanks by incisions, is observed in the central part of the pockmarks in
515 the Ligurian margin and in the western flank of the Corsica Trough (Fig. 14a,b). The deformation,
516 elongation and erosion in all the observed pockmarks is consistent with the local current direction
517 provided by the hydrodynamic model: bottom currents flow westwards along the slope along the
518 Ligurian margin (Fig. 5); southwards along the western flank of the Corsica Trough (Fig. 7a); towards
519 the northwest in the zone of pockmarks on the eastern flank of the Pianosa Ridge (Fig. 7a) and in the
520 southern part of a seamount in the Northern Tyrrhenian Sea (Fig. 13a,b).
521

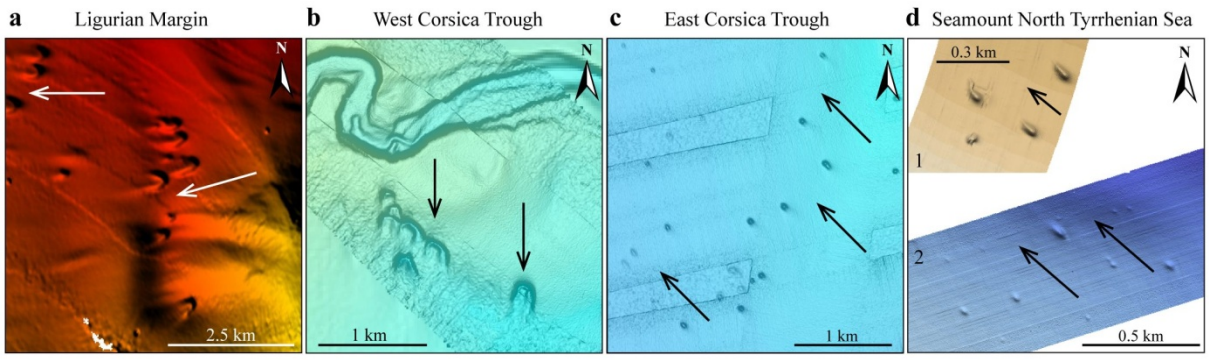

522
523 **Fig. 14.** Multibeam bathymetry of elongated pockmarks in: (a) the Ligurian Margin, (b) in the western
524 flank of the Corsica Trough, (c) in the eastern flank of the Corsica Trough, and (d) at the south of the

seamount in the Northern Tyrrhenian Sea. Arrows indicate direction of dominant bottom currents. See locations in Figs. 5d, 7b and 13a, respectively.

5. Discussion

5.1. The role of currents in sediment redistribution and sediment source of contourites

The MENOR hydrodynamic model shows the presence of two cyclonic gyres in the Corsica Trough that affect the whole water column. One gyre is located between the latitudes 42°30'N and 42°50'N, and the other is located between 42°N and 42°30'N (Fig. 15). The Corsica Trough is a small confined basin where turbidity currents and contouritic processes are dominant on opposite basin flanks (Miramontes et al., 2016). The eastern flank of the Corsica Trough (the Pianosa Ridge) is a sediment-starved slope, with little direct sediment supply from the adjacent continental shelf, littoral zone and continent (Roveri et al., 2002). In contrast, the western slope of the Corsica Trough is dominated by turbidity currents (Gervais et al., 2006) originated from several turbidite systems: Golo, Tavignano and Fiume-Orbo (Bellaiche et al., 1994). Hemipelagic and turbiditic deposits are dominant on the western slope, whereas contouritic deposits along the eastern slope (Cattaneo et al., 2014; Miramontes et al., 2016).

An open question is the possible sediment source for contouritic deposit, but given the morphological confinement of the Corsica Trough, it is plausible that the fine sediment fraction transported in suspension by turbidity currents may be ponded within the basin, pirated by alongslope flows and transported by bottom currents to other zones of the basin, particularly during sea level low-stands, when the turbidite system is active (Calvès et al., 2013; Toucanne et al., 2015). The cyclonic gyres modelled in the Corsica Trough could be a very effective mechanism of transport for the fine sedimentary fraction carried in suspension from the western flank to the eastern flank of the Corsica Trough. The fine-grained sediment would be finally deposited on the large muddy contourite drifts along the Pianosa Ridge.

The drifts of the Balearic and Ligurian Seas are probably also formed in part by sediment carried by turbidity currents through abundant canyons and channels on the slopes (Figs. 2 and 5). Figure 3 shows two turbidite channels in the centre of the Minorca basin, the Valencia Channel and Blanes Canyon~~hannels~~. The Valencia Channel routes a network of submarine canyons from the eastern Iberian margin and is the main conduit of sediment transport to the deep Liguro-Provençal basin (Amblas et al., 2011). The sediment carried by turbidity currents is probably transported by bottom currents and deposited in the contourite systems along the Iberian and Minorca slopes. In the Ligurian Sea, contourite drifts are located on ridges between canyons ~~interfluves~~ and are probably often fed by overbanking downslope processes (Fig. 5).

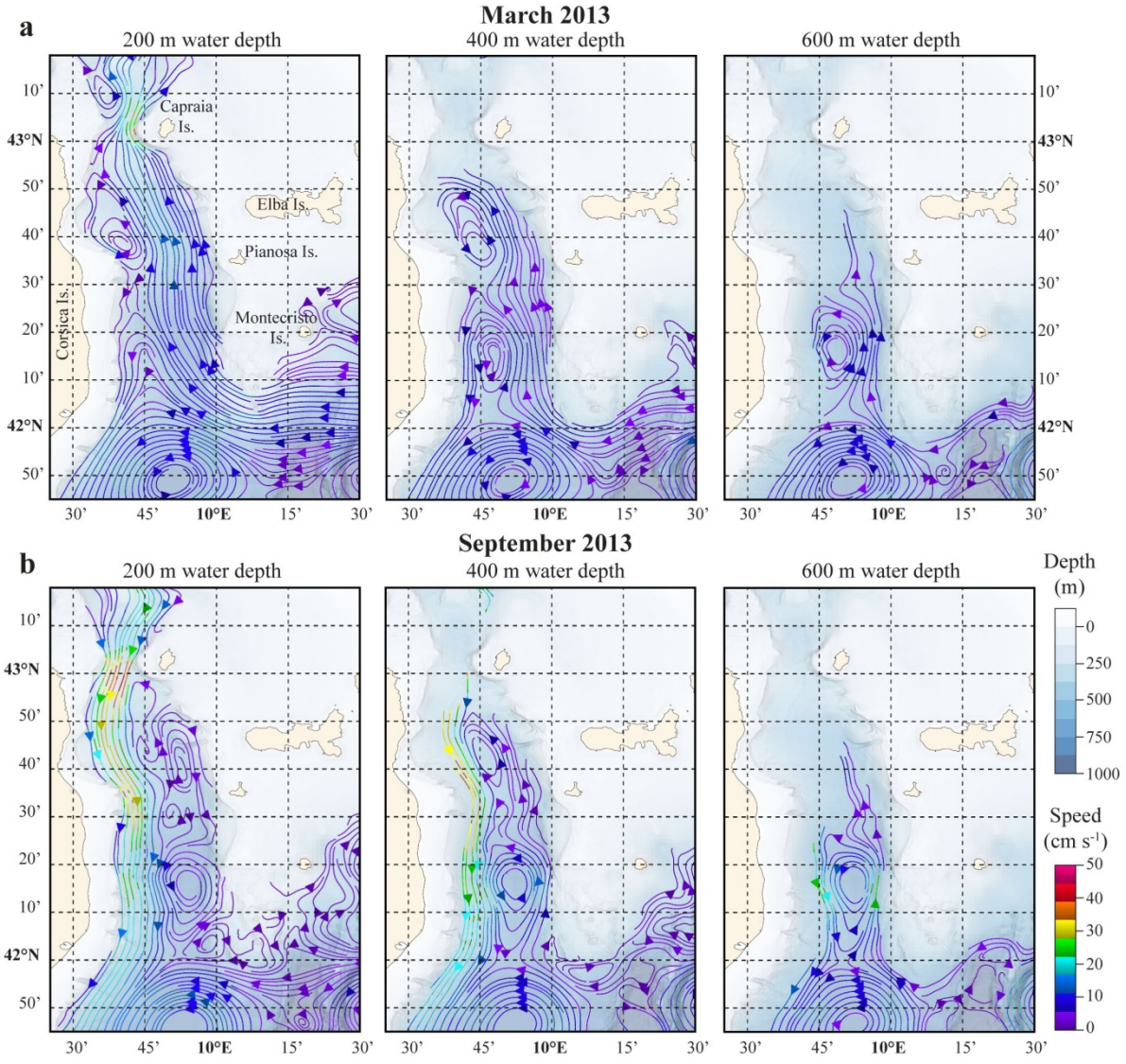

Fig. 15. Stream lines of the mean currents at three different depths: 200, 400 and 600 m calculated with the 400 m zoom of the MENOR model during (a) March 2013 and (b) September 2013; and bathymetry map. Note the presence of cyclonic gyres in the basin at all depths and seasons.

5.2. Seasonal variability in circulation and the impact of extreme events

The results of the hydrodynamic model show that the areas identified from seismic and bathymetric data as foci for erosion (e.g. moats and eroded continental slopes) present P90 BSS during winter that exceeded the critical shear stress required to erode unconsolidated mud (above 0.05 $N \cdot m^{-2}$; Schaaff et al., 2002) (Table 3; Fig. 16a). In some cases P90 BSS was even higher than the critical shear stress of erosion of fine sand (above 0.1 $N \cdot m^{-2}$, according to the Shields curve; Soulsby, 1997) (Table

572 3; Fig. 16a). Durrieu de Madron et al. (2017) observed local sediment resuspension during the major
573 winter open-ocean convection events and estimated that the critical BSS of fine and medium silts in
574 the Liguro-Provençal basin ranges between the 0.04 and 0.13 $N \cdot m^{-2}$. In contrast, during summer the
575 areas identified as foci for erosion typically present much lower P90 BSS and thus may not always be
576 under erosive conditions (Table 3; Fig. 16a). If we consider acceptable the assumption that winter
577 2013 conditions could be considered as a proxy for oceanographic conditions during cold periods
578 (glaciations), then the eroded features observed in the geophysical data could be the result of
579 erosion due to more vigorous bottom currents during colder climatic periods. Even if sediment is
580 deposited during warm climatic periods in these areas (when shear stresses are lower), it is probably
581 removed during cold climatic periods, resulting in net erosion or in a lower sediment accumulation.
582

Zone	Environment	Mean speed winter ($cm \cdot s^{-1}$)	90th percentile BSS-winter ($N \cdot m^{-2}$)	Mean speed summer ($cm \cdot s^{-1}$)	90th percentile BSS-summer ($N \cdot m^{-2}$)
1	Minorca moat	10	0.10	8-9	0.03-0.06
1	Minorca slope	17-24	0.20-0.34	14-20	0.10-0.20
1	Minorca drift	5-7	0.02-0.03	6-7	0.01-0.02
1	Iberian moat	11-13	0.07-0.1	5-6	0.02
1	Iberian slope	18-20	0.20-0.30	8-9	0.03-0.04
1	Iberian reworked levee	5-7	0.02-0.03	3-4	0.005-0.01
2	Portofino moat	15-17	0.14-0.18	11-12	0.06-0.08
2	Portofino drift	9-10	0.05-0.07	5-7	0.017-0.02
3	Pianosa moats	8-10	0.05	5	0.02-0.04
3	Shelf edge-plastered drift	10-12	0.05-0.13	4	0.01
3	Shelf edge-offshore Pianosa Island	13-17	0.13-0.23	4-6	0.02-0.04
3	Plastered drift	6-8	0.03-0.05	4	0.01
3	Separated mounded drift	7-10	0.05-0.07	5-7	0.02-0.03
3	Multicrested drift	7-11	0.05-0.10	4-8	0.02-0.05
3	Upper slope multicrested drift	7-9	0.04-0.07	4-5	0.01
3	Foot of the slope north Elba Canyon	10	0.1	6-7	0.03-0.05

583 **Table 3.** Mean speed and 90th percentile of the Bottom Shear Stress (P90 BSS) computed during
584 winter and summer 2013 in the three study areas: (1) Balearic Sea; (2) Ligurian Sea; (3) Northern
585 Tyrrhenian Sea. The areas classified as depositional environments (according to geophysical data) are
586 in grey colour, while the erosive environments are in white colour.
587

588 The Minorca slope is subject to vigorous currents, between 14 and 24 $cm \cdot s^{-1}$, that are capable of
589 eroding sand continuously (Table 3; Figs. 2, 3, 16a). This is supported, over longer time scales, by
590 geophysical evidence of truncations on the slope (Figs. 3 and 4a). Zones of deposition (identified
591 from geophysical data) are only found in areas of lower current velocity, but the unconsolidated mud

592 can also be eroded during enhanced bottom circulation during cold periods (Fig. 16b). Overall,
593 sediment can be deposited and eroded several times before being definitively incorporated into the
594 sediment record. Features such as contourite moats would likely have been continuously under
595 erosion during sea level low-stands. A similar approach has been proposed for the Gulf of Cadiz
596 (Llave et al., 2006, 2007; Hernández-Molina et al., 2006, 2014) and the South Atlantic (Preu et al.,
597 2013). Thran et al. (2018) also deduced in a global scale that contourite deposition is caused by high-
598 energy intermittent events.
599

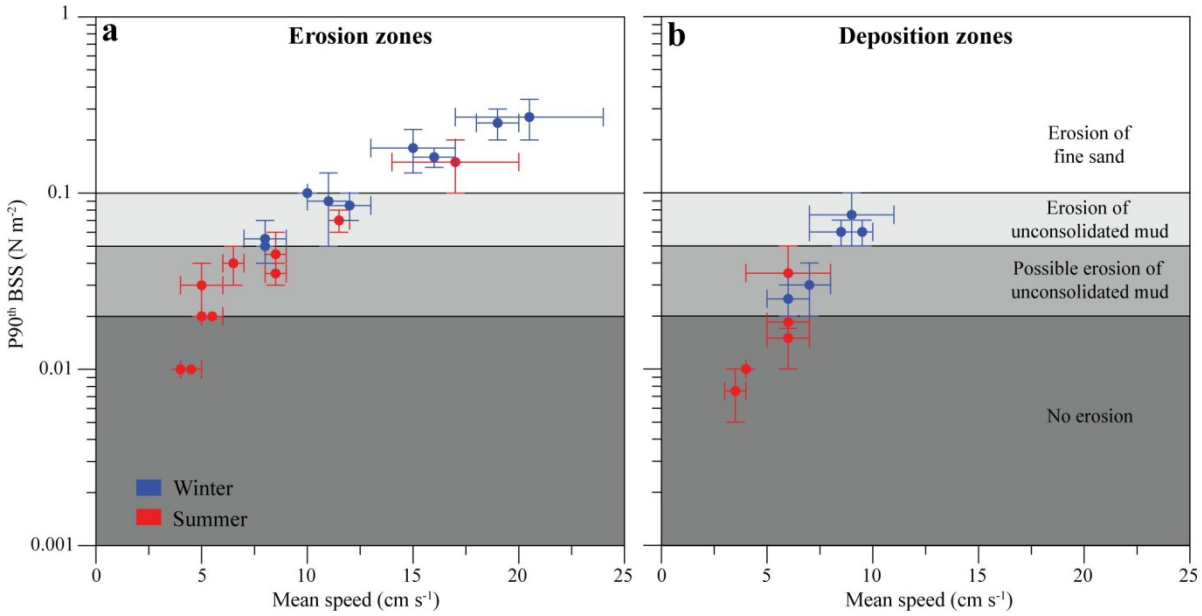

600

601 **Fig. 16.** Plot of the mean speed and 90th percentile of the Bottom Shear Stress (BSS) calculated with
602 the MENOR model for the period of winter and summer 2013 in the zones previously classified
603 according the geophysical data as zones of erosion or sediment deposition, detailed in Table 3. The
604 critical shear stress for erosion is based on a critical BSS for unconsolidated mud ranging between
605 0.02 and 0.05 $N \cdot m^{-2}$ (Schaff et al., 2002) and a critical BSS for fine sand of 0.1 $N \cdot m^{-2}$ according to the
606 Shields curve (Soulsby, 1997).
607
608
609

610 5.3. Conceptual implications for continental margin morphology

611 Adams and Schlager (2000) and O'Grady et al. (2000) proposed a classification of modern margins
612 and observed that a sigmoidal slope profile is the most common margin morphology (about 50% of
613 the studied margins). Sigmoidal margins consist of a convex upper part and a concave lower part that
614 is below the point of maximum slope (O'Grady et al., 2000). This type of shape is characteristic of
615 margins with plastered drifts along continental slopes (Figs. 10; 17; Fauguères et al., 1999; Rebesco
616 et al., 2014; Principaud et al., 2015; Tournadour et al., 2015). Multiple contouritic terraces and
617 plastered drifts can be associated at different depths in a margin, such as in the Argentinean and
618 Uruguayan margins (Preu et al., 2013; Hernández-Molina et al., 2016), corresponding to the stepped
619 margin in the classification of O'Grady et al. (2000). Deep bottom currents can thus have a very
620 important influence in the morphology of continental margins at large scale, as proposed by Mosher
621 et al. (2017), and they should be taken into account in the analysis of the origin of continental slope
622 curvature.

623 In the NW Mediterranean Sea, three main types of margin morphology can develop, depending on
624 the amount of sediment supply and on the distribution of the bottom-current velocities (Fig. 17). In
625 all the described zones, the whole water column flows in the same direction. We identified: Type 1) a
626 starved margin with an eroded continental slope and a separated elongated mounded drift at the
627 foot of the slope; Type 2) a margin with direct sediment supply and a homogeneous bottom-current
628 distribution, resulting in smooth regular seafloor; Type 3) a starved margin with heterogeneous
629 bottom current distribution, resulting in the formation of a plastered drift on the slope and a
630 separated elongated mounded drift at the foot of the slope. This classification attempts to relate
631 bottom-current characteristics to sediment drift morphology and configuration in order to
632 diagnostically identify current regime for other contourite features worldwide.

633 Type 1: A separated elongated mounded drift develops at the foot of the slope when bottom
634 currents are vigorous along the lower slope and they become weaker basinwards, allowing the
635 formation of a drift. Enhanced bottom currents at the foot of the slope generate a moat and may

laterally induce the formation of deposits with a mounded shape, such as in the Minorca slope (Fig. 3). This particular setting would be characteristic of starved margins with little direct sediment supply from the mainland and the shelf, but with lateral supply of the fine-grained sediment by the currents. Moreover, the action of vigorous bottom currents on the slope can easily erode unconsolidated sediment and prevent sediment deposition in this area (Fig. 17a). Contourite features formed at the seamount of the Northern Tyrrhenian Sea are developed in similar conditions. They are related to escarpments with little sediment accumulation on the slope, and the drifts grow in a zone of lower bottom currents along the foot of the slope (Fig. 13). These drifts have a small size compared to the Minorca drift because they are related to obstacles and confined by seafloor irregularities, while in the case of Minorca the contourites develop all along the margin. Faugères et al. (1999) and Rebesco et al. (2014) suggested that separated elongated mounded drifts are associated with steep slopes, generally located on the lower slope and are formed due to a high current speed gradient, in agreement with our observations and modelled currents.

Type 2: In a slope where sediment is directly supplied by gravitational processes and is also affected by coeval active and strong bottom currents, the resulting morphology is a smooth regular seafloor with a progradational sedimentary stacking pattern, such as the western flank of the Corsica Trough (Fig. 8). Dominant downslope processes and a high sedimentation rate could mask the influence of bottom currents. The most important factor in the generation of mounded sedimentary morphologies is the heterogeneous distribution of bottom currents, since the sediment would preferentially accumulate in the zone of weak currents. If currents are even across the slope, either weak or vigorous, there would be no zone of preferential accumulation and thus no mounded morphology (Fig. 17b). This type of gently sloped margins is typical of regions with high sediment input (O'Grady et al., 2000).

Type 3: Well-developed plastered drifts can be found on starved margins with heterogeneous bottom-current distribution. Plastered drifts are typically convex-shaped sedimentary bodies that have an oval shape in plan view, like in the Pianosa Ridge (Figs. 9 and 10). Here, they develop in a

zone of weak bottom currents confined between two zones of faster bottom currents in the upper and in the distal part of the lower slope, resulting in the formation of a terrace upslope and a moat downslope (Fig. 17c). Moreover, the direction of bottom currents on the middle of the plastered drift is mainly across slope, favouring the sediment accumulation in this area. Related to a zone of slow bottom currents at the foot of the slope, a separated elongated mounded drift can develop in a similar way to Type 1 features (Fig. 17a).

The association of plastered drift in the slope and separated elongated mounded drift at the foot of the slope has been observed in other settings, such as the Alboran Sea (Ercilla et al., 2016) and the Uruguayan margin (Hernández-Molina et al., 2016). Plastered drifts with a convex shape can cover most of the slope and strongly influence the slope morphology (Principaud et al., 2015; Tournadour et al., 2015; Ercilla et al., 2016; Miramontes et al., 2016). In the study area, the formation of plastered drifts can be explained by the distribution of geostrophic currents on the slope (Fig. 17c): strong bottom currents in the upper and lower part of the plastered drifts prevent sediment deposition in these areas, while sedimentation mainly occurs in the central part of the plastered drifts where bottom currents are slow (Fig. 9). If a pycnocline is located on the terrace (as modelled in the Pianosa Ridge, Fig. 8c), the action of internal waves could enhance sediment erosion on the terrace, at the top of the plastered drift (Hernández-Molina et al., 2009; Preu et al., 2013).

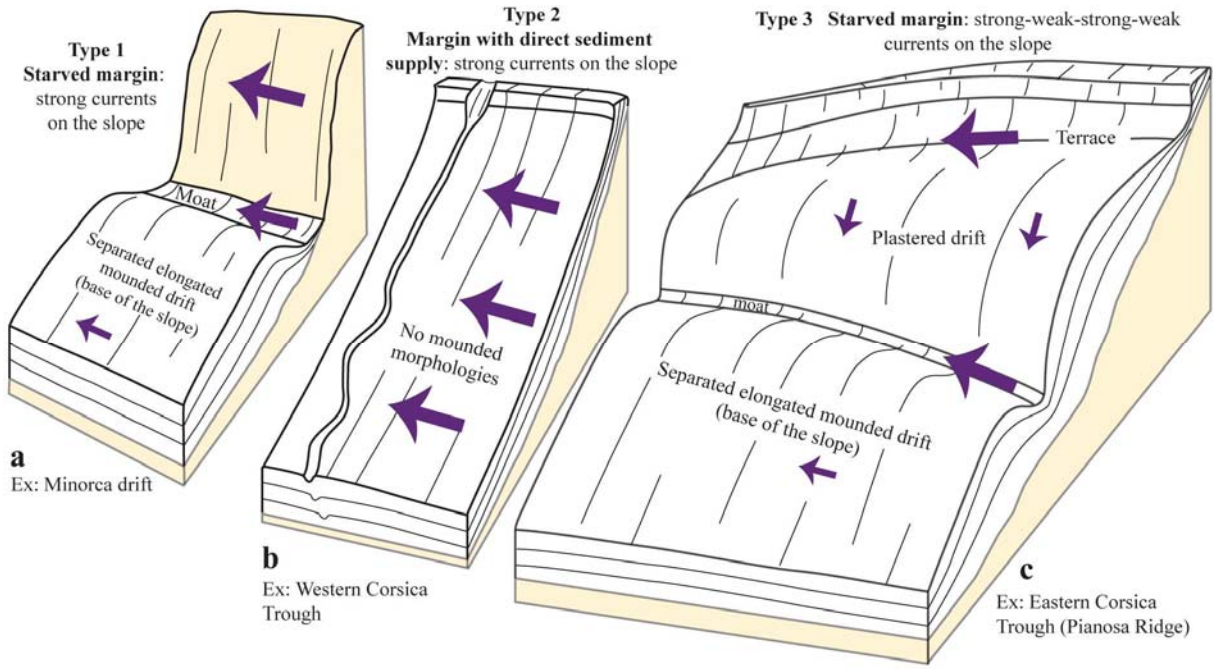

679

680 **Fig. 17.** 3D schematics showing three different types of continental slopes: (a) Type 1: a starved
681 margin with an eroded continental slope and separated elongated mounded drift at the foot of the
682 slope; (b) Type 2: a continental slope with direct sediment supply and a homogeneous bottom-
683 current distribution; (c) Type 3: a starved continental slope with heterogeneous bottom current
684 distribution, resulting in the formation of a plastered drift on the slope and a separated elongated
685 mounded drift at the foot of the slope. The arrows indicate bottom current direction and intensity
686 according to their size.

687

688 **6. Conclusions**

689 In spite of the potentially large gap in the chronological range of investigation - namely days to
690 decades for physical oceanography and years to millions of years for sedimentology - we observe
691 close agreement between the results of hydrodynamic modelling focussed at the seafloor and the
692 distribution of contourite drifts and their morphological elements in three sectors of the
693 Mediterranean Sea. The main conclusions of this study can be summarised as follows:

(1) The results of the MARS3D hydrodynamic model in the MENOR configuration are consistent with the morphology of contourites observed in three areas of the NW Mediterranean Sea: the Balearic Sea, the Ligurian Sea and the Northern Tyrrhenian Sea.

(2) By coupling the model results of winter 2013 and summer 2013 with the geophysical and sedimentological data, we suggest that events of more intense circulation are controlling the formation and evolution of moats and erosive features on the seafloor. During warm climatic periods (characterised by weak currents), fine-grained sediment could be deposited in some of these areas, but during cold climatic periods the enhanced bottom currents would generate erosion, resulting in net erosion. Therefore, the preservation potential of deposits along these erosional features is very low.

(3) The presence of gyres in confined basins with asymmetric sediment input causes the redistribution of sediment from the margin with a direct sediment supply to the opposite starved margin.

(4) The development of mounded sedimentary morphologies is favoured by heterogeneous bottom current distributions. The plastered drifts analysed in this study are formed in zones of relative low current velocity, mainly with an across-slope (oblique and/or perpendicular) direction, confined between zones of high alongslope current velocity. These morphologies are commonly observed in starved margins not affected by frequent downslope gravity flows. Separated elongated mounded drifts are formed in zones of low bottom currents at the foot of the slope associated with fast currents on the slope. In contrast, when bottom currents are homogeneous across the margin (either fast or slow), no mounded shapes can develop and the seafloor regularly deepens toward the basin.

These results provide a high resolution physical oceanographic framework to improve our understanding of palaeoceanographic conditions for the formation of contourite depositional systems. Our results provide useful guidance for the interpretation of flow regimes and sedimentary facies distribution based on the seafloor morphology found in other bottom-current dominated deep-marine settings. Further studies and new numerical modelling should be performed in other

areas for determining more conceptual implications, especially about the interplay of different oceanographic processes in the formation of contourite features, and about the effects of sea-level fluctuations on bottom currents.

Acknowledgments

We would like to thank the captains and the crews of the WestMedFlux2 cruise in 2018 onboard the R/V L'Atalante, PAMELA-PAPRICA and PRISME2 cruises onboard R/V L'Atalante, PRISME3 cruise onboard the R/V Pourquoi pas? in 2013, SIGOLO cruise in 2008 onboard the R/V Le Suroît, CORFAN cruise in 1998 onboard the R/V L'Europe and CORFAN 2 cruise in 1999 onboard the R/V Le Suroît and. We are grateful to Kevin Samalens for his help with the data from the Ligurian Margin. We acknowledge CINES for BULL Occigen computer access (project ode7663). We also thank LabexMer and Ifremer for having awarded E. Miramontes with a travel grant during her stay at the Royal Holloway University of London. We acknoweldge GALSI Spa for donation of seismic and bathymetric data. The fellowship of E. Miramontes and the cruise PRISME2-PAPRICA were co-funded by TOTAL and Ifremer as part of the PAMELA (Passive Margins Exploration Laboratories) scientific project. The PAMELA project is a scientific project led by Ifremer and TOTAL in collaboration with Université de Bretagne Occidentale, Université Rennes 1, Université Pierre and Marie Curie, CNRS and IFPEN. The research was supported through the projects CTM2016-75129-C3-2-R and CGL2016-80445-R (AEI/FEDER, UE). The research of F.J Hernández-Molina was conducted in the framework of the "*The Drifters Research Group*" of the Royal Holloway University of London (UK) and it is related to the projects CTM 2012-39599-C03, CGL2016-80445-R, and CTM2016-75129-C3-1-R. M.A. Clare was supported by the NERC Environmental Risks to Infrastructure Innovation Programme (NE/N012798/1) and NERC National Capability project Climate Linked Atlantic Sector Science Programme (CLASS). We thank the two anonymous reviewers for helping us to improve the final version of the manuscript.

746 **References**

747 Adams, E.W., Schlager, W., 2000. Basic types of submarine slope curvature. Journal of Sedimentary
748 Research 70, 814-828.

749 Albérola, C., Millot, C., Font, J., 1995. On the seasonal and mesoscale variabilities of the Northern
750 Current during the PRIMO-0 experiment in the Western Mediterranean Sea. Oceanologica Acta
751 18, 163–192.

752 Amblas, D., Gerber, T.P., Canals, M., Pratson, L.F., Urgeles, R., Lastras, G., Calafat, A.M., 2011.
753 Transient erosion in the Valencia Trough turbidite systems, NW Mediterranean
754 Basin. Geomorphology 130, 173-184.

755 Artale, V., Astraldi, M., Buffoni, G., Gasparini, G.P., 1994. Seasonal variability of gyre-scale circulation
756 in the northern Tyrrhenian Sea. Journal of Geophysical Research: Oceans 99, 14127-14137.

757 Astraldi, M., Gasparini, G.P., 1992. The seasonal characteristics of the circulation in the north
758 Mediterranean basin and their relationship with the atmospheric-climatic conditions. Journal of
759 Geophysical Research: Oceans 97, 9531-9540.

760 Astraldi, M., Gasparini, G.P., et Sparnocchia, S., 1994. The seasonal and interannual variability in the
761 Ligurian-Provencal Basin. Coastal and Estuarine Studies, 93-113.

762 Bellacicco, M., Anagnostou, C., Falcini, F., Rinaldi, E., Tripsanas, K., Salusti, E., 2016. The 1987 Aegean
763 dense water formation: A streamtube investigation by comparing theoretical model results,
764 satellite, field, and numerical data with contourite distribution. Marine Geology 375, 120-133.

765 Bellaiche, G., Droz, L., Gaullier, V., Pautot, G., 1994. Small submarine fans on the eastern margin of
766 Corsica: sedimentary significance and tectonic implications. Marine Geology 117, 177-185.

767 Bonaldo, D., Benetazzo, A., Bergamasco, A., Campiani, E., Foglini, F., Sclavo, M., Trincardi, F., Carniel,
768 S., 2016. Interactions among Adriatic continental margin morphology, deep circulation and
769 bedform patterns. Marine Geology 375, 82-98.

770 Cacho, I., Grimalt, J.O., Sierro, F.J., Shackleton, N., Canals, M., 2000. Evidence for enhanced
771 Mediterranean thermohaline circulation during rapid climatic coolings. Earth and Planetary
772 Science Letters 183, 417-429.
773 Calvès, G., Toucanne, S., Jouet, G., Charrier, S., Thereau, E., Etoubleau, J., Marsset, T., Droz, L., Bez,
774 M., Abreu, V., 2013. Inferring denudation variations from the sediment record; an example of the
775 last glacial cycle record of the Golo Basin and watershed, East Corsica, western Mediterranean
776 sea. Basin Research 25, 197-218.
777 Cattaneo, A., 2013a. PRISME2 cruise, RV L'Atalante, http://dx.doi.org/10.17600/13010050.
778 Cattaneo, A., 2013b. PRISME3 cruise, RV Pourquoi pas ?, http://dx.doi.org/10.17600/13030060.
779 Cattaneo, A., Jouet, G., 2013. PAMELA-PAPRICA cruise, RV L'Atalante,
780 http://dx.doi.org/10.17600/13010300.
781 Cattaneo, A., Jouet, G., Charrier, S., Thereau, E., Riboulot, V., 2014. Submarine landslides and
782 contourite drifts along the Pianosa Ridge (Corsica Trough, Mediterranean Sea). In: Krastel, S. (Ed.),
783 Submarine mass movements and their consequences 37. Springer, Dordrecht, pp. 435–445..
784 Cattaneo, A., Miramontes, E., Samalens, K., Garreau, P., Caillaud, M., Marsset, B., Corradi, N.,
785 Migeon, S., 2017. Contourite identification along Italian margins: The case of the Portofino drift
786 (Ligurian Sea). Marine and Petroleum Geology 87, 137-147.
787 Ciuffardi, T., Napolitano, E., Iacono, R., Reseghetti, F., Raiteri, G., Bordone, A., 2016. Analysis of
788 surface circulation structures along a frequently repeated XBT transect crossing the Ligurian and
789 Tyrrhenian Seas. Ocean Dynamics 66, 767-783.
790 Da Silva, J. C. B., New, A. L., Magalhaes, J. M., 2009. Internal solitary waves in the Mozambique
791 Channel: Observations and interpretation. Journal of Geophysical Research: Oceans 114,
792 https://doi.org/ 10.1029/2008JC005125.
793 de Lavergne, C., Madec, G., Capet,X., Guillaume Maze, G., Roquet, F., 2016. Getting to the bottom of
794 the ocean. Nature Geosciences 9, 857-858.

795 Duhaut, T., Honnorat, M., Debreu, L., 2008. Développements numériques pour le modèle MARS.
796 Technical Report. PREVIMER report - Ref: 06/2 210 290.
797 Durrieu de Madron, X., Houpert, L., Puig, P., Sanchez-Vidal, A., Testor, P., Bosse, A., Estournel, C.,
798 Somot, S., Bourrin, F., Bouin, M.N., Beauverger, M., Beguery, L., Calafat, A., Canals, M., Cassou, C.,
799 Coppola, L., Dausse, D., D'Ortenzio, F., Font, J., Heussner, S., Kunesch, S., Lefevre, D., Le Goff, H.,
800 Martín, J., Mortier, L., Palanques, A., Raimbault, P., 2013. Interaction of dense shelf water
801 cascading and open-sea convection in the northwestern Mediterranean during winter 2012.
802 Geophysical Research Letters 40, 1379-1385.
803 Durrieu de Madron, X., Ramondenc, S., Berline, L., Houpert, L., Bosse, A., Martini, S., Guidi, L., Conan,
804 P., Curtil, C., Delsaut, N., Kunesch, S., Ghiglione, J.F., Marsaleix, P., Pujo-Pay, M., Séverin, T.,
805 Testor, P., Tamburini, C., the ANTARES collaboration, 2017. Deep sediment resuspension and thick
806 nepheloid layer generation by open-ocean convection. Journal of Geophysical Research: Oceans
807 122(3), 2291-2318.
808 Dutkiewicz, A., Müller, R. D., Hogg, A. M., Spence, P., 2016. Vigorous deep-sea currents cause global
809 anomaly in sediment accumulation in the Southern Ocean. Geology 44(8), 663-666.
810 Ercilla, G., Juan, C., Hernández-Molina, F. J., Bruno, M., Estrada, F., Alonso, B., Casas, D., Farran, M.,
811 Llave, E., García, M., Vázquez, J. T., D'Acremont,E., Gorini, C., Palomino, D., Valencia, J., El
812 Moumni, B., Ammar A., 2016. Significance of bottom currents in deep-sea morphodynamics: an
813 example from the Alboran Sea. Marine Geology 378, 157-170.
814 Estournel, C., Testor, P., Damien, P., D'Ortenzio, F., Marsaleix, P., Conan, P., Kessouri, F., Durrieu de
815 Madron, X., Coppola, L., Lellouche, J.-M., Belamari, S., Mortier, L., Ulses, C., Bouin, M.-N., Prieur, L.
816 2016. High resolution modeling of dense water formation in the north-western Mediterranean
817 during winter 2012–2013: Processes and budget. Journal of Geophysical Research: Oceans 121,
818 5367–5392.
819 Faugères, J. C., Stow, D. A. V, Imbert, P., Viana, A., 1999. Seismic features diagnostic of contourite
820 drifts. Marine Geology 162, 1–38.

821 Faugères, J.-C., Stow, D.A.V., 2008. Contourite drifts: nature, evolution and controls. In: Rebesco, M.,
822 Camerlenghi, A. (Eds.), Contourites. Developments in Sedimentology, 60. Elsevier, Amsterdam, pp.
823 257–288.
824 Font, J., Salat, J., Tintoré, J., 1988. Permanent features of the circulation in the Catalan Sea.
825 Oceanologica acta 9, 51–57.
826 Gardner, W.D., Tucholke, B.E., Richardson, M.J., Biscaye, P.E., 2017. Benthic storms, nepheloid layers,
827 and linkage with upper ocean dynamics in the western North Atlantic. Marine Geology 385, 304-
828 327.
829 Gasparini, G. P., Zodiatis, G., Astraldi, M., Galli, C., Sparnocchia, S., 1999. Winter intermediate water
830 lenses in the Ligurian Sea. Journal of Marine Systems 20, 319-332.
831 Gervais, A., Savoye, B., Mulder, T., Gonthier, E., 2006. Sandy modern turbidite lobes: A new insight
832 from high resolution seismic data. Marine and Petroleum Geology 23, 485-502.
833 Hernández-Molina, F.J., Llave, E., Stow, D.A.V., García, M., Somoza, L., Vázquez, J.T., Lobo, F.J.,
834 Maestro, A., Díaz del Río, V., León, R., Medialdea, T., Gardner, J., 2006. The contourite
835 depositional system of the Gulf of Cádiz: A sedimentary model related to the bottom current
836 activity of the Mediterranean outflow water and its interaction with the continental margin. Deep
837 Sea Research Part II: Topical Studies in Oceanography 53, 1420-1463.
838 Hernández-Molina, F.J., Llave, E., Stow, D.A.V., 2008. Continental slope contourites. In: Rebesco, M.,
839 Camerlenghi, A. (Eds.), Contourites. Developments in Sedimentology, 60. Elsevier, Amsterdam, pp.
840 379–408.
841 Hernández-Molina, F. J., Paterlini, M., Violante, R., Marshall, P., de Isasi, M., Somoza, L., Rebesco, M.,
842 2009. Contourite depositional system on the Argentine Slope: an exceptional record of the
843 influence of Antarctic water masses. Geology 37, 507-510.
844 Hernández-Molina, F.J., Stow, D.A.V., Alvarez-Zarikian, C.A., Acton, G., Bahr, A., Balestra, B.,
845 Ducassou, E., Flood, R., Flores, J.-A., Furota, S., Grunert, P., Hodell, D., Jimenez-Espejo, F., Kim, J.K.,
846 Krissek, L., Kuroda, J., Li, B., Llave, E., Lofi, J., Lourens, L., Miller, M., Nanayama, F., Nishida, N.,

847 Richter, C., Roque, C., Pereira, H., Goni, M.F.S., Sierro, F.J., Singh, A.D., Sloss, C., Takashimizu, Y.,
848 Tzanova, A., Voelker, A., Williams, T., Xuan, C., 2014. PALEOCEANOGRAPHY Onset of
849 Mediterranean outflow into the North Atlantic. Science 344, 1244-1250.
850 Hernández-Molina, F. J., Soto, M., Piola, A. R., Tomasini, J., Preu, B., Thompson, P., Badalini, G.,
851 Creaser, A., Violante, R.A., Morales, E., Paterlini, M., De Santa Ana, H., 2016. A contourite
852 depositional system along the Uruguayan continental margin: Sedimentary, oceanographic and
853 paleoceanographic implications. Marine Geology 378, 333-349.
854 Hunter, S., Wilkinson, D., Louarn, E., McCave, I. N., Rohling, E., Stow, D. A., Bacon, S., 2007. Deep
855 western boundary current dynamics and associated sedimentation on the Eirik Drift, Southern
856 Greenland Margin. Deep Sea Research Part I: Oceanographic Research Papers 54, 2036-2066.
857 Knutz, P.C., 2008. Paleoceanographic Significance of Contourite Drifts. In: Rebesco, M., Camerlenghi,
858 A. (Eds.), Contourites. Developments in Sedimentology, 60. Elsevier, Amsterdam, pp. 457–516.
859 Laberg, J.S., Camerlenghi, A., 2008. The significance of contourites for submarine slope stability. In:
860 Rebesco, M., Camerlenghi, A. (Eds.), Contourites. Developments in Sedimentology, 60. Elsevier,
861 Amsterdam, pp. 537-556.
862 Lascaratos, A., Williams, R.G., Tragou, E., 1993. A mixed-layer study of the formation of levantine
863 intermediate water. Journal of Geophysical Research 98, 14 739–14 749.
864 Lascaratos, A., Roether, W., Nittis, K., Klein, B., 1999. Recent changes in deep water formation and
865 spreading in the eastern Mediterranean Sea: a review. Progress in Oceanography 44, 5-36.
866 Lazure, P., Dumas, F., 2008. An external-internal mode coupling for a 3D hydrodynamical model for
867 applications at regional scale (MARS). Advances in Water Resources 31, 233-250.
868 Léger, F., Lebeaupin Brossier, C., Giordani, H., Arsouze, T., Beuvier, J., Bouin, M.-N., Bresson, E.,
869 Ducrocq, V., Fourrié, N., Nuret, M., 2016. Dense water formation in the north-western
870 Mediterranean area during HyMeX-SOP2 in 1/36° ocean simulations: Sensitivity to initial
871 conditions. Journal of Geophysical Research: Oceans 122, 5549-5569.

872 Leroux, E., Rabineau, M., Aslanian, D., Gorini, D. Molliex, S., Bache, F., Robin, C., Droz, L., Moulin, M.,
873 Poort, J., Rubino, J.-L., Suc, J.P, 2017. High resolution evolution of terrigenous sediment yields in
874 the Provence Basin during the last 6 Ma: relation with climate and tectonics. Basin Research 29(3),
875 305-339.
876 Llave, E., Schönfeld, J., Hernández-Molina, F.J., Mulder, T., Somoza, L., Díaz del Río, V., Sánchez-
877 Almazo, I., 2006. High-resolution stratigraphy of the Mediterranean outflow contourite system in
878 the Gulf of Cadiz during the late Pleistocene: The impact of Heinrich events. Marine Geology 227,
879 241-262.
880 Llave, E., Hernández-Molina, F.J., Somoza, L., Stow, D.A.V., Díaz Del Río, V.D., 2007. Quaternary
881 evolution of the contourite depositional system in the Gulf of Cadiz. Geological Society, London,
882 Special Publications 276, 49-79.
883 Lüdmann, T., Wiggershaus, S., Betzler, C., Hübscher, C., 2012. Southwest Mallorca Island: a cool-
884 water carbonate margin dominated by drift deposition associated with giant mass
885 wasting. Marine Geology 307, 73-87.
886 Mauffret, A., 1988. VALSIS 2 cruise, RV Jean Charcot, http://dx.doi.org/10.17600/88003211.
887 McCave, I.N., 2008. Size sorting during transport and deposition of fine sediments: Sortable silt and
888 flow speed. In: Rebesco, M., Camerlenghi, A. (Eds.), Contourites. Developments in Sedimentology,
889 60. Elsevier, Amsterdam, pp. 121–142.
890 McWilliams, J.C., 2016. Submesoscale currents in the ocean. Proc. R. Soc. A. 472, 20160117.
891 Millot, C., 1999. Circulation in the Western Mediterranean Sea. Journal of Marine Systems 20, 423-
892 442.
893 Millot, C., 2009. Another description of the Mediterranean Sea outflow. Progress in Oceanography
894 82, 101-124.
895 Millot, C., Taupier-Letage, I., 2005. Circulation in the Mediterranean sea. The Mediterranean Sea.
896 Springer, pp. 29-66.

897 Minto'o, C.M.A., Bassetti, M.A., Morigi, C., Ducassou, E., Toucanne, S., Jouet, G., Mulder, T., 2015.
898 Levantine intermediate water hydrodynamic and bottom water ventilation in the northern
899 Tyrrhenian Sea over the past 56,000 years: new insights from benthic foraminifera and ostracods.
900 Quaternary International 357, 295–313.
901 Miramontes, E., Cattaneo, A., Jouet, G., Théreau, E., Thomas, Y., Rovere, M., Cauquil, E., Trincardi, F.,
902 2016. The Pianosa Contourite Depositional System (Northern Tyrrhenian Sea): Drift morphology
903 and Plio-Quaternary stratigraphic evolution. Marine Geology 378, 20-42.
904 Miramontes, E., Garziglia, S., Sultan, N., Jouet, G., Cattaneo, A., 2018. Morphological control of slope
905 instability in contourites: A geotechnical approach. Landslides 15(6), 1085-1095.
906 Mosher, D. C., Campbell, D. C., Gardner, J. V., Piper, D. J. W., Chaytor, J. D., Rebesco, M., 2017. The
907 role of deep-water sedimentary processes in shaping a continental margin: The Northwest
908 Atlantic. Marine Geology 393, 245-259.
909 Nielsen, T, Knutz, P.C., Kuijpers, A., 2008. Seismic Expression of Contourite Depositional Systems. In:
910 Rebesco, M., Camerlenghi, A. (Eds.), Contourites. Elsevier, pp. 301-321.
911 O'Grady, D. B., Syvitski, J. P., Pratson, L. F., Sarg, J. F., 2000. Categorizing the morphologic variability
912 of siliciclastic passive continental margins. Geology 28, 207-210.
913 Palanques, A., Puig, P., Durrieu de Madron, X. D., Sánchez-Vidal, A., Pasqual, C., Martín, J., Calafat, A.,
914 Heussner, S., Canals, M., 2012. Sediment transport to the deep canyons and open-slope of the
915 western Gulf of Lions during the 2006 intense cascading and open-sea convection period.
916 Progress in Oceanography 106, 1-15.
917 Picard, K., Radke, L.C., Williams, D.K., Nicholas, W.A., Siwabessy, P.J., Floyd, J.F.H., Gafeira, J.,
918 Przeslawski, R., Huang, Z., Nichol, S. (2018). Origin of high density seabed pockmark fields and
919 their use in inferring bottom currents. Geosciences, 8, 195.
920 Pinardi, N., Arneri, E., Crise, A., Ravaioli, M., Zavatarelli, M., 2006. The physical, sedimentary and
921 ecological structure and variability of shelf areas in the Mediterranean Sea. In: Robinson, A., Brink,
922 K. (Eds.), The Sea 14. Harvard University Press, pp. 1243-1330.

923 Pinardi, N., Zavatarelli, M., Adani, M., Coppini, G., Fratianni, C., Oddo, P., Simoncelli, S., Tonani, M.,
924 Lyubarstsev, V., Dobrici, S., Bonaduce, A., 2015. Mediterranean Sea large-scale low-frequency
925 ocean variability and water mass formation rates from 1987 to 2007: A retrospective analysis.
926 Progress in Oceanography 132, 318-332.
927 Pinot, J.M., López-Jurado, J.L., Riera, M., 2002. The CANALES experiment (1996-1998). Interannual,
928 seasonal, and mesoscale variability of the circulation in the Balearic Channels. Progress in
929 Oceanography 55(3-4), 335-370.
930 Poort, J., Gorini, C., 2018. WESTMEDFLUX-2 cruise, RV L'Atalante,
931 https://doi.org/10.17600/18000402
932 Preu, B., Hernandez-Molina, F.J., Violante, R., Piola, A.R., Paterlini, C.M., Schwenk, T., Voigt, I.,
933 Krastel, S., Spiess, V., 2013. Morphosedimentary and hydrographic features of the northern
934 Argentine margin: The interplay between erosive, depositional and gravitational processes and its
935 conceptual implications. Deep-Sea Research Part I-Oceanographic Research Papers 75, 157-174.
936 Principaud, M., Mulder, T., Gillet, H., Borgomano, J., 2015. Large-scale carbonate submarine mass-
937 wasting along the northwestern slope of the Great Bahama bank (Bahamas): Morphology,
938 architecture, and mechanisms. Sedimentary Geology 317, 27-42.
939 Rabineau, M., Leroux, E., Aslanian, D., Bache, F., Gorini, C., Moulin, M., Molliex, S., Droz, L., Reis, A.D.,
940 Rubino, J.-L., Guillocheau, F., Olivet, J.-L., 2014. Quantifying subsidence and isostatic readjustment
941 using sedimentary paleomarkers, example from the Gulf of Lions. Earth Planetary Science Letters
942 388, 1-14.
943 Rebesco, M., Camerlenghi, A., 2008. Contourites. Developments in Sedimentology 60. Elsevier 663
944 pp.
945 Rebesco, M., Hernández-Molina, F.J., Van Rooij, D.,Wåhlin, A., 2014. Contourites and associated
946 sediments controlled by deep-water circulation processes: State-of-the-art and future
947 considerations. Marine Geology 352, 111-154.

948 Riboulot, V., Thomas, Y., Berné, S., Jouet, G., Cattaneo, A., 2014. Control of Quaternary sea-level
949 changes on gas seeps. Geophysical Research Letters 41(14), 4970-4977.
950 Roveri, M., 2002. Sediment drifts of the Corsica Channel, Northern Tyrrhenian Sea. In: Stow, D.A.V.,
951 Pudsey, C.J., Howe, J.A., Faugères, J.-C., Viana, A.R. (Eds.), Deep-Water Contourite Systems.
952 Modern Drifts and Ancient Series, Seismic and Sedimentary Characteristics. Geological Society,
953 London, Memoirs 22, pp. 191–208.
954 Rubio, A., Taillandier, V., Garreau, P., 2009. Reconstruction of the Mediterranean northern current
955 variability and associated cross-shelf transport in the Gulf of Lions from satellite-tracked drifters
956 and model outputs. Journal of Marine Systems 78, S63-S78.
957 Salat, J., Font, J., 1987. Water mass structure near and offshore the Catalan coast during the winters
958 of 1982 and 1983. Annales geophysicae 5B, 49–54.
959 Savoye, B., 1998. CORFAN cruise, RV L'Europe, http://dx.doi.org/10.17600/98060110.
960 Savoye, B., 2001. CORFAN 2 cruise, RV Le Suroît, http://dx.doi.org/10.17600/1020030.
961 Savoye, B., 2008. SIGOLO cruise, RV Le Suroît, http://dx.doi.org/10.17600/8020110.
962 Schaaff, E., Grenz, C., Pinazo, C., 2002. Erosion of particulate inorganic and organic matter in the Gulf
963 of Lion. Comptes Rendus Geoscience 334, 1071–1077.
964 Schattner, U., Lazar, M., Souza, L.A.P., ten Brink, U., Mahiques, M.M., 2016. Pockmark asymmetry
965 and seafloor currents in the Santos Basin offshore Brazil. Geo-Marine Letters 36(6), 457-464.
966 Schlichting, H., 1962. Boundary Layer Theory. 6th ed., McGraw-Hill, New York, 744 pp.
967 Shanmugam, G., 2013. Modern internal waves and internal tides along oceanic pycnoclines:
968 Challenges and implications for ancient deep-marine baroclinic sands. AAPG bulletin, 97, 799-843.
969 Soulet, Q., Migeon, S., Gorini, C., Rubino, J.L., Raisson, F., Bourges, P., 2016. Erosional versus
970 aggradational canyons along a tectonically-active margin: The northeastern Ligurian margin
971 (western Mediterranean Sea). Marine Geology 382, 17-36.
972 Soulsby, R.L., 1997. Dynamics of marine sands. A manual for practical applications. Thomas Telford,
973 London, 249 pp.

974 Stow, D.A.V., Kahler, G., Reeder, M., 2002. Fossil contourites: type example from an Oligocene
975 palaeoslope system, Cyprus. In: Stow, D.A.V., Pudsey, C.J., Howe, J.A., Faugères, J.-C., Viana, A.R.
976 (Eds.), Deep-water Contourite Systems: Modern Drifts and Ancient Series, Seismic and
977 Sedimentary Characteristics. Geological Society, London, Memoir 22, pp. 443–455.
978 Stow, D.A.V., Hernández-Molina, F.J., Llave, E.,Sayago-Gil, M., Díaz del Río, V., Branson, A., 2009.
979 Bedform-velocity matrix: the estimation of bottom current velocity from bed form observations.
980 Geology 37, 327–330.
981 Thran, A.C., Dutkiewicz, A., Spence, P., Müller, R.D., 2018. Controls on the global distribution of
982 contourite drifts: Insights from an eddy-resolving ocean model. Earth and Planetary Science
983 Letters 489, 228-240.
984 Toucanne, S., Jouet, G., Ducassou, E., Bassetti, M.A., Dennielou, B., Minto'o, C.M.A., Lahmi, M.,
985 Touyet, N., Charlier, K., Lericolais, G., Mulder, T., 2012. A 130,000-year record of Levantine
986 Intermediate Water flow variability in the Corsica Trough, western Mediterranean Sea.
987 Quaternary Science Reviews 33, 55-73.
988 Toucanne, S., Angue Minto'o, C.M., Fontanier, C., Bassetti, M.A., Jorry, S.J., Jouet, G., 2015. Tracking
989 rainfall in the Northern Mediterranean borderlands during sapropel deposition. Quaternary
990 Science Reviews 129, 178–195.
991 Tournadour, E., Mulder, T., Borgomano, J., Hanquiez, V., Ducassou, E. Gillet, H., 2015. Origin and
992 architecture of a Mass Transport Complex on the northwest slope of Little Bahama Bank
993 (Bahamas): Relations between off-bank transport, bottom current sedimentation and
994 submarine landslides. Sedimentary Geology 317, 9-26.
995 Vandorpe, T.P., Van Rooij, D., Stow, D.A.V., Henriet, J.-P., 2011. Pliocene to Recent shallow-water
996 contourite deposits on the shelf and shelf edge off south-western Mallorca, Spain. Geo-Marine
997 Letters 31, 391-403.

998 Velasco, J.P.B., Baraza, J., Canals, M., Balón, J., 1996. La depression periférica y el lomo contourítico
999 de Menorca: evidencias de la actividad de corrientes de fondo al N del talud Balear. Geogaceta 20,
1000 359–362.
1001 Viana, A.R., 2008. Economic Relevance of Contourites. In: Rebesco, M., Camerlenghi, A. (Eds.),
1002 Contourites. Elsevier, pp. 491-510.
1003 Vignudelli, S., Cipollini, P., Astraldi, M., Gasparini, G. P., Manzella, G., 2000. Integrated use of
1004 altimeter and in situ data for understanding the water exchanges between the Tyrrhenian and
1005 Ligurian Seas. Journal of Geophysical Research: Oceans 105, 19649–19663.
1006 Zhang, W.Y., Hanebuth, T.J.J., Stober, U., 2016. Short-term sediment dynamics on a meso-scale
1007 contourite drift (off NW Iberia): Impacts of multi-scale oceanographic processes deduced from the
1008 analysis of mooring data and numerical modelling. Marine Geology 378, 81-100.